Systems/Circuits

PSA-NCAM Colocalized with Cholecystokinin-Expressing Cells in the Hippocampus Is Involved in Mediating Antidepressant Efficacy

Jun Yamada,[1] Chihiro Sato,[2] Kohtarou Konno,[3] Masahiko Watanabe,[3] and Shozo Jinno[1]

[1]Department of Anatomy and Neuroscience, Graduate School of Medical Sciences, Kyushu University, Fukuoka 812-8582, Japan, [2]Laboratory of Animal Cell Function, Bioscience and Biotechnology Center, Nagoya University, Nagoya 464-8601, Japan, and [3]Department of Anatomy, Hokkaido University Graduate School of Medicine, Sapporo 060-8638, Japan

The extracellular glycan polysialic acid linked to neural cell adhesion molecule (PSA-NCAM) is principally expressed in the developing brain and the adult neurogenic regions. Although colocalization of PSA-NCAM with cholecystokinin (CCK) was found in the adult brain, the role of PSA-NCAM remains unclear. In this study, we aimed to elucidate the functional significance of PSA-NCAM in the CA1 region of the male mouse hippocampus. Combined fluorescence *in situ* hybridization and immunohistochemistry showed that few vesicular glutamate transporter 3-negative/CCK-positive ($VGluT3^-/CCK^+$) cells were colocalized with PSA-NCAM, but most of the $VGluT3^+/CCK^+$ cells were colocalized with PSA-NCAM. The somata of PSA-NCAM $^+/CCK^+$ cells were highly innervated by serotonergic boutons than those of PSA-NCAM $^-/CCK^+$ cells. The expression ratios of 5-HT_{3A} receptors and p11, a serotonin receptor-interacting protein, were higher in PSA-NCAM $^+/CCK^+$ cells than in PSA-NCAM $^-/CCK^+$ cells. Pharmacological digestion of PSA-NCAM impaired the efficacy of antidepressant fluoxetine (FLX), a selective serotonin reuptake inhibitor, but not the efficacy of benzodiazepine anxiolytic diazepam. A Western blot showed that restraint stress decreased the expressions of p11 and mature brain-derived neurotrophic factor (BDNF), and FLX increased them. Interestingly, the FLX-induced elevation of expression of p11, but not mature BDNF, was impaired by the digestion of PSA-NCAM. Quantitative reverse transcription-polymerase chain reaction showed that restraint stress reduced the expression of polysialyltransferase ST8Sia IV and FLX elevated it. Collectively, PSA-NCAM colocalized with VGluT3 $^+/CCK^+$ cells in the CA1 region of the hippocampus may play a unique role in the regulation of antidepressant efficacy via the serotonergic pathway.

Key words: antidepressant; cholecystokinin; GABAergic neuron; hippocampus; PSA-NCAM

Significance Statement

Polysialic acid (PSA) is composed of eight or more α2,8-linked sialic acids. Here, we examined the functional significance of polysialic acid linked to the neural cell adhesion molecule (PSA-NCAM) in the adult mouse hippocampus. Few vesicular glutamate transporter 3-negative/cholecystokinin-positive ($VGluT3^-/CCK^+$) cells were colocalized with PSA-NCAM, but most of the $VGluT3^+/CCK^+$ cells were colocalized with PSA-NCAM. The expression ratios of 5-HT_{3A} receptors and p11, a serotonin receptor-interacting protein, were higher in PSA-NCAM$^+/CCK^+$ cells than in PSA-NCAM$^-/CCK^+$ cells. The efficacy of antidepressants, but not anxiolytics, was impaired by the digestion of PSA-NCAM. The antidepressant-induced increase in p11 expression was inhibited following PSA-NCAM digestion. We hence hypothesize that PSA-NCAM colocalized with $VGluT3^+/CCK^+$ cells may play a unique role in regulating antidepressant efficacy.

Introduction

Polysialic acid (PSA) is a large extracellular glycan composed of eight or more α2,8-linked sialic acids (Schnaar et al., 2014) linked to the neural cell adhesion molecule (NCAM). Previous studies have reported that the polysialylated form of NCAM (PSA-NCAM) is highly expressed in the developing brain (Rutishauser, 2008) and the adult neurogenic regions (Seki, 2002). It has also

Received July 25, 2019; revised Oct. 30, 2019; accepted Nov. 25, 2019.

Author contributions: J.Y. and S.J. designed research; J.Y. performed research; J.Y. analyzed data; J.Y. wrote the first draft of the paper; C.S., K.K., M.W., and S.J. contributed unpublished reagents/analytic tools; S.J. edited the paper; S.J. wrote the paper.

This work was supported in part by the Japan Society for the Promotion of Science (KAKENHI Grants 16K18379 and 19K06924 to J.Y., and Grants 19H05022, 15H04267, and 19K22812 to S.J.). We thank Machiko Endoh for secretarial assistance, Kana Maekawa for technical assistance, and Editage (www.editage.jp) for English language editing.

The authors declare no competing financial interests.

Correspondence should be addressed to Shozo Jinno at sjnno@med.kyushu-u.ac.jp.

https://doi.org/10.1523/JNEUROSCI.1779-19.2019

been shown that PSA-NCAM (or NCAM) is expressed in non-neurogenic regions of the adult brain. The immunoreactivity for NCAM is found along the plasma membrane of aspiny interneurons in the caudate nucleus of adult rodents (DiFiglia et al., 1989). Further, aspiny interneurons are shown to be immunoreactive for cholecystokinin (CCK) in the caudate and putamen of adult cats (Adams and Fisher, 1990). Interestingly, previous studies have suggested that PSA-NCAM may be associated with serotonergic and dopaminergic neurotransmission in the cortex of adult rats (Sairanen et al., 2007; Castillo-Gómez et al., 2008). In addition, PSA-NCAM may be somewhat implicated in the regulation of neuronal plasticity in the adult vertebrate brain (Rutishauser, 2008). Despite these studies, the significance of PSA-NCAM in the adult brain remains unclear.

In the cortex and hippocampus of the adult rodent brain, PSA-NCAM is mainly colocalized with CCK-positive (CCK^+) cells (Nacher et al., 2002; Gómez-Climent et al., 2011). CCK was initially isolated from gastrointestinal tissues but later found in various regions of the CNS (Beinfeld, 1983). It has now been established that almost all CCK^+ cells belong to GABAergic inhibitory neurons in the hippocampus (Nunzi et al., 1985). Moreover, CCK^+ cells in the hippocampus are shown to receive serotonergic terminals, which activate CCK^+ cells through 5-HT_3 receptors (Armstrong and Soltesz, 2012). Interestingly, the postsynaptic targets of CCK^+ cells are enriched with the α2 subunit of $GABA_A$ receptors, which regulate anxiety-related behaviors (Freund, 2003). It has thus been suggested that CCK^+ cells expressing 5-HT receptors may be involved in the regulation of mood and emotional behavior (McLaughlin et al., 2014).

In the mouse hippocampus, CCK^+ cells represent 5–10% of GABAergic neurons (Jinno and Kosaka, 2006). According to the morphological and electrophysiological characteristics, CCK^+ cells have been divided into several subtypes in the hippocampus (Cope et al., 2002). Vesicular glutamate transporter 3 (VGluT3) and vasoactive intestinal protein (VIP) are shown to be subtype-specific markers of hippocampal CCK^+ cells (Somogyi et al., 2004). CCK^+ cell-firing contributes to differentiating subgroups of pyramidal cells, forming neuronal assemblies in the hippocampus (Klausberger et al., 2005). Although several subtype-specific functions of CCK^+ cells have been found in the hippocampal microcircuits (Del Pino et al., 2017), the details are not fully elucidated.

In this study, we aimed to clarify the functional significance of PSA-NCAM colocalized with CCK^+ cells in the CA1 region of the mouse hippocampus. The vast majority of $VGluT3^+/CCK^+$ cells were colocalized with PSA-NCAM. The somata of PSA-$NCAM^+/CCK^+$ cells were highly innervated by serotonergic terminals than those of PSA-NCAM-negative (PSA-$NCAM^-$)/CCK^+ cells. The efficacy of the antidepressant fluoxetine (FLX), but not anxiolytic diazepam (DZP), was impaired by the pharmacological digestion of PSA-NCAM. Our results indicate that PSA-NCAM colocalized with $VGluT3^+/CCK^+$ cells may play a unique role in the regulation of antidepressant efficacy via the serotonergic pathway.

Materials and Methods

Animals. In all, 134 male C57BL/6J mice (8–12 weeks old, 20–25 g; CLEA) were used in this study. The animals were housed with a 12 h light/12 h dark cycle and fed *ad libitum* on a standard rodent chow (CE-2; CLEA). The Committee of Ethics on Animal Experiments in the Graduate School of Medical Sciences, Kyushu University, approved every procedure.

Experimental groups. The mice were divided into multiple groups according to the predetermined procedures, and a summary of the experimental groups is as follows.

A total of 16 mice were used for the combined fluorescence *in situ* hybridization (FISH) and immunohistochemistry only: naive mice (n = 8); vehicle-treated mice (n = 4); mice treated with endo-α-*N*-acylneuraminidase (Endo-N), an enzyme that specifically removes the PSA moiety associated with NCAM (n = 4).

A total of 78 mice were used for the experiment combining restraint stress and the selective serotonin reuptake inhibitor antidepressant FLX. Animals were treated with intrahippocampal injection of vehicle (n = 39) or Endo-N (n = 39), then divided into three groups: nonstressed control mice (NS mice, n = 26); mice exposed to restraint stress (R-S mice, n = 26); mice treated with FLX following restraint stress (R-F mice, n = 26).

A total of 40 mice were used for the experiment combining fear conditioning and the benzodiazepine anxiolytic DZP. The animals were treated with an intrahippocampal injection of vehicle (n = 20) or Endo-N (n = 20), then divided into two groups: mice treated with fear conditioning and saline (F-S mice, n = 20); mice treated with fear conditioning and DZP (F-D mice, n = 20). The same animal groups were also tested with an elevated plus-maze.

Purification of enzyme. The soluble form of Endo-N was purified from lysates of K1F-infected *Escherichia coli* by modifying previously published procedures (Hallenbeck et al., 1987). The unit of Endo-N was determined by using penta-*N*-acetylneuraminic acid (Neu5Ac) as a substrate. The amount of mono-Neu5Ac and tetra-Neu5Ac produced at 37°C for 1 min was measured since Endo-N requires a minimum of five sialyl residues (DP5, where DP represents the degree of polymerization) for activity.

Intrahippocampal injection of Endo-N. Mice were anesthetized with an intraperitoneal injection (i.p.) of sodium pentobarbital (50 mg/kg) and mounted onto a stereotaxic frame. Endo-N (20 U/ml) or saline was injected bilaterally into four sites (0.5 μl/site, eight sites in total) targeting the CA1 region with positive pressure using a glass micropipette (inside diameter, 20–30 μm). The coordinates of four injection sites were as follows: (1) 1.84 mm posterior to the bregma, 1.0 mm lateral from the midline, and 1.50 mm below the pial surface; (2) 1.84 mm posterior to the bregma, 1.2 mm lateral from the midline, and 1.35 mm below the pial surface; (3) 2.18 mm posterior to the bregma, 1.2 mm lateral from the midline, and 1.35 mm below the pial surface; and (4) 2.18 mm posterior to the bregma, 1.5 mm lateral from the midline, and 1.35 mm below the pial surface.

Administration of FLX and DZP. The antidepressant FLX or anxiolytic DZP was administered in different animals as follows. FLX (20 mg/kg, i.p.; Tokyo Chemical Industry) or vehicle (saline, 5 mg/kg, i.p.) was administered for 8 consecutive days. DZP (0.5 mg/kg, i.p.; FUJIFILM Wako Pure Chemical Corporation) or vehicle (saline, 5 ml/kg, i.p.) was administered 30 min before behavioral testing for 3 consecutive days.

Perfusion fixation. Mice were deeply anesthetized with an overdose of sodium pentobarbital (120 mg/kg, i.p.), and perfused transcardially with phosphate-buffered saline (PBS, pH 7.4), followed by 4% paraformaldehyde in 0.1 M phosphate buffer. The brains were left *in situ* for 2–3 h at room temperature and then removed from the skull. The brains were cut coronally on a vibrating microtome (VT1000S; Leica Microsystems) into 40-μm-thick sections. All sections were processed in the free-floating condition.

FISH. Sections were subjected to prehybridization for 1 h by incubation in a hybridization buffer [50% formamide, 50 mM Tris-HCl, pH 7.5, 0.02% Ficoll, 0.02% polyvinylpyrrolidone, 0.02% bovine serum albumin (BSA), 0.6 mM NaCl, 200 μg/ml transfer RNA, 1 mM ethylenediaminetetraacetic acid (EDTA), and 10% dextran sulfate]. The following riboprobes, which were labeled with either fluorescein (FITC) or digoxigenin (DIG), were used for the hybridization reaction: mouse VGluT3 (bases 22–945; NCBI Reference Sequence NM_182959) and mouse CCK (bases 124–411; NCBI Reference Sequence NM_031161). Hybridization was performed at 64°C for 12 h in a hybridization buffer supplemented with complementary RNA probes (1:1000). After washing with saline-sodium citrate buffer, the sections were incubated in NaCl-Tris-EDTA (NTE)

buffer for 20 min, 20 mM iodoacetamide in NTE buffer for 20 min, and Tris-NaCl-Tween (TNT) buffer for 20 min. The sections were incubated with a peroxidase-conjugated anti-DIG antibody (1:1000; Roche Diagnostics; RRID:AB_514500) for 1 h, to detect DIG. After washing with TNT buffer, fluorescence detection was performed using a cyanine 3 (Cy3)-TSA plus amplification kit (PerkinElmer). After the inactivation of residual peroxidase activity by treating sections in 1% H_2O_2 for 30 min, the second detection was performed by incubating sections with a peroxidase-conjugated anti-FITC antibody (1:1000; Roche Diagnostics; RRID:AB_840257), followed by incubation with the FITC-TSA plus amplification kit (PerkinElmer).

Immunohistochemistry. Sections that had been processed for FISH were postfixed with 4% paraformaldehyde for 30 min at room temperature. After washing with PBS, the sections were blocked with 1.0% BSA in PBS containing 0.3% Triton X-100 and 0.05% sodium azide for 3 h at 4°C. After blocking, the sections were incubated for 5 d at 4°C with a mixture of appropriately selected primary antibodies: mouse monoclonal anti-CCK (1:10000; gift from CURE/Gastroenteric Biology Center; Antibody/RIA Core; RRID:AB_10013360), mouse monoclonal anti-PSA-NCAM (1:1000; AbCys SA; RRID:AB_2313692), mouse polyclonal anti-glutamic acid decarboxylase (GAD) (1:10000; Sigma-Aldrich; RRID:AB_261978), mouse monoclonal anti-p11 (1:1000; R&D Systems; RRID:AB_2183467), rabbit polyclonal anti-GAD antibody (1:10000; Sigma-Aldrich, RRID:AB_259920), rabbit polyclonal anti-proCCK (1:5000; Frontier Institute; RRID:AB_2571674), rabbit polyclonal anti-S100β (1:20000; Sigma-Aldrich; RRID:AB_1856538), rabbit polyclonal anti-vesicular glutamate transporter 1 (VGluT1) (1:10000; Frontier Institute; RRID:AB_2571616), rabbit polyclonal anti-vesicular monoamine transporter 2 (VMAT2) (1:10000; Frontier Institute; RRID:AB_2571857), rabbit polyclonal anti-VIP (1:1000; ImmunoStar; RRID:AB_572270), goat polyclonal anti-p11 (1:1000; R&D Systems; RRID:AB_2254166), goat polyclonal anti-5-HT_{3A} receptor antibody (1:1000; Abcam; RRID:AB_869956) goat polyclonal anti-sex-determining region Y-box 2 (Sox2) (1:2000; Santa Cruz Biotechnology; RRID:AB_661259), guinea pig polyclonal anti-doublecortin (DCX) (1:10000; Millipore; RRID:AB_1586992), and guinea pig polyclonal anti-VGluT3 (1:10000; Frontier Institute; RRID:AB_2571855).

After washing with PBS, the sections were incubated with a mixture of appropriately selected fluorescence-labeled secondary antibodies (Jackson ImmunoResearch) including aminomethylcoumarin (AMCA)-conjugated donkey anti-rabbit IgG (1:500), FITC-conjugated donkey anti-rabbit IgG (1:500), FITC-conjugated donkey anti-guinea pig IgG (1:500), Cy3-conjugated donkey anti-goat IgG (1:500), and Alexa Fluor 647-conjugated donkey anti-mouse IgG (1:500) for 12 h at 4°C. Selected sections were counterstained with nucleic acid–binding fluorescent dye, YOYO-1 (1:1000; Thermo Fisher Scientific). After washing with PBS, the sections were mounted with Vectashield (Vector Laboratories).

Optical disector analysis of the PSA-NCAM. To analyze the spatial distributions of PSA-NCAM in the CA1 region of the hippocampus, we conducted the following optical disector analyses.

A total of four naive mice were used to analyze the expression patterns of PSA-NCAM, proCCK, and CCK mRNA. The same animals were also used to analyze the expression patterns of PSA-NCAM, VIP, VGluT3 mRNA, and CCK mRNA. Four sections were selected from each animal for the combined FISH and immunohistochemistry.

A total of 12 mice treated with vehicle (NS mice, $n = 4$; R-S mice, $n = 4$; R-F mice, $n = 4$) and 12 mice treated with Endo-N (NS mice, $n = 4$; R-S mice, $n = 4$; R-F mice, $n = 4$) were used to analyze the patterns of expression of PSA-NCAM, VGluT3 mRNA, and CCK mRNA. Four sections, from each animal, were selected for combined FISH and immunohistochemistry.

One stack of optical sections containing the CA1 region was captured using an optical sectioning microscope (Apotome.2; Carl Zeiss) equipped with a dry objective lens [×20, numerical aperture (NA) 0.8]. An unbiased counting frame (71.5 × 71.5 μm) (Gundersen and Jensen, 1987) was superimposed on optical sections with the Blend Images plugin of ImageJ 1.46 (RRID:SCR_003070). Densities were then estimated as follows:

$$\text{Density} = \Sigma Q^- / [h \times a(fra)/\text{SV}]$$

where ΣQ^- is the number of disector-counted cells, h is the optical disector height, $a(fra)$ is the total area of the counting frames, and SV is the volumetric shrinkage factor (0.65) (Jinno et al., 1998).

Optical disector analysis of the adult hippocampal neurogenesis. A total of eight mice were used to examine the spatial distributions of adult hippocampal neurogenesis-related cells by the optical disector analysis (vehicle-treated mice, $n = 4$; Endo-N-treated mice, $n = 4$). Two sections, from each animal, were selected for the immunostaining of S100β, Sox2, and DCX.

One stack of optical sections containing the dentate gyrus was captured using an optical sectioning microscope (Apotome.2; Carl Zeiss) equipped with a dry objective lens (×20, NA 0.8). A two-cell-thick zone (40 μm), between the border of the granule cell layer and the hilus, was defined as the subgranular zone. Considering the efficiency, we counted all cells distributed in this narrow area without using the counting frame. The area of the granule cell layer was estimated using the image analysis software package ImageJ 1.46 according to the point-counting technique (Gundersen et al., 1988). The densities were calculated as follows:

$$\text{Density} = \Sigma Q^- / [h \times a(gl)/\text{SV}]$$

where ΣQ^- is the number of disector-counted cells, h is the optical disector height, $a(gl)$ is the area of the granule cell layer, and SV is the volumetric shrinkage factor (0.65) (Jinno et al., 1998).

Colocalization analysis. To quantify the molecular colocalization at the cellular level, we counted the numbers of cells expressing the following combinations of molecules: (1) 5-HT_{3A} receptor, VGluT3 mRNA, and CCK mRNA; (2) p11 and PSA-NCAM; and (3) p11 and 5-HT_{3A} receptor. A total of four naive mice were used in the colocalization analysis. From each animal, three sections were selected for immunohistochemistry, FISH, or both.

One stack of optical sections containing the CA1 region was captured using an optical sectioning microscope (Apotome.2; Carl Zeiss) equipped with a dry objective lens (×20, NA 0.8). The number of cells distributed in the CA1 region was manually counted by ImageJ 1.46.

Line profile analysis. A total of 12 mice were used to examine the densities of the synaptic boutons covering the somata of CCK^+ cells (naive mice, $n = 4$; vehicle-treated mice, $n = 4$; Endo-N-treated mice, $n = 4$). Four sections were selected from each animal for the combined FISH and immunohistochemistry.

One stack of optical sections containing the CA1 region was captured using an optical sectioning microscope (Apotome.2; Carl Zeiss) equipped with an oil-immersion objective lens (×63, NA 1.40). Lines (2 μm long), perpendicular to the soma, were drawn around the whole circumferential surface of the CCK^+ cells at 2-μm intervals, and the pixel intensities along the paths were measured by ImageJ 1.46. Information, from differential interference contrast (DIC) and fluorescence images, was combined to identify the soma outline. Approximately 30 lines were obtained from each CCK^+ cell. We analyzed the molecular profile of the path within 2 μm from the soma to count the synaptic boutons, as reported previously (Yamada et al., 2017).

Areal fluorescence intensity analysis. Eight total mice were used to examine the extent of PSA-NCAM digestion by local injection of Endo-N into the CA1 region (vehicle-treated mice, $n = 4$; Endo-N-treated mice, $n = 4$). Three sections, from each animal, were selected for the immunohistochemistry.

Eight-bit images, containing the entire area of the hippocampus, were obtained using a widefield fluorescence microscope (Axio Scope.A1; Carl Zeiss) equipped with a dry objective lens (×5, NA 0.15). The outline of the CA1 region and dentate gyrus were traced with the freehand-segment tool of ImageJ 1.46, and the gray level for PSA-NCAM in each area was measured. The exposure time, gain, and offset were computed to ensure a high signal while avoiding saturation. All section images were captured in the same manner.

Single-cell fluorescence intensity analysis. A total of 15 mice were used to examine the single-cell fluorescence intensity of PSA-NCAM (NS mice, $n = 5$; R-S mice, $n = 5$; R-F mice, $n = 5$). Four sections were selected from each animal for immunostaining.

In total, 18 mice were used to analyze the single-cell fluorescence intensity of p11: nine mice treated with vehicle (NS mice, $n = 3$; R-S mice, $n = 3$; R-F mice, $n = 3$) and nine mice treated with Endo-N (NS mice,

$n = 3$; R-S mice, $n = 3$; R-F mice, $n = 3$). Three sections, from each animal, were selected for the immunohistochemistry.

One stack of optical sections containing the CA1 region was captured using an optical sectioning microscope (Apotome.2; Carl Zeiss) equipped with a dry objective lens (×20, NA 0.8). The ellipse circumscribing the single soma was traced manually, and the gray level for PSA-NCAM or p11 was measured by using ImageJ 1.46). Out-of-focus somata were excluded from the measurement. The exposure time, gain, and offset were computed to ensure a high signal but to avoid saturation. All section images were captured in the same manner.

Digestion of PSA-NCAM and the efficacy of FLX. A total of 60 mice were used to examine the potential effects of PSA-NCAM digestion on the antidepressant efficacy of FLX: 30 mice treated with vehicle (NS mice, $n = 10$; R-S mice, $n = 10$; R-F mice, $n = 10$) and 30 mice treated with Endo-N (NS mice, $n = 10$; R-S mice, $n = 10$; R-F mice, $n = 10$).

One day after the injection of vehicle or Endo-N, mice were placed in a ventilated transparent plastic tube (3 cm in diameter and 12 cm in length) and subjected to 2 h-long restraint stress for 12 consecutive days. The holes in the head and along the sidewall of the tube enabled airflow. Mice could move their heads and anterior limbs but could not move their posterior limbs or turn their bodies around. During the restraint period, mice did not have access to food or water. The administration of FLX started 7 d after the injection, and the treatment continued for 8 d.

Fifteen days after the injection of vehicle or Endo-N, mice were evaluated by the open-field test. The animals were placed in a square open-field chamber (50 × 50 × 50 cm; Muromachi Kikai) for 10 min and allowed to move freely. The center of the field was illuminated at 100 lux. The center area size was designated as 30 × 30 cm, and an entry was recorded whenever 50% of a mouse's body entered the center of the field. The distance traveled and time spent (in the center area and the outer zone) were automatically measured using a computer-assisted data acquisition system, ANY-maze (Stoelting; RRID:SCR_014289).

During the second day of open field testing, the depression-related behavior was evaluated by the forced swim test. Mice were forced to swim for 6 min in an acrylic cylinder (20 × 20 × 25 cm) containing 15 cm water at 25°C. Both the distances traveled and immobility time during the final 4 min of the 6 min test period were measured using ANY-maze (Stoelting). Immobility was defined as a period of at least 1 s with no active behavior. After the swimming session, each mouse was dried, warmed, and returned to the home cage.

Digestion of PSA-NCAM and the efficacy of DZP. In total, 40 mice were used to examine the potential effects of PSA-NCAM digestion on the anxiolytic efficacy of DZP: 20 mice treated with vehicle (F-S mice, $n = 10$; F-D mice, $n = 10$) and 20 mice treated with Endo-N (F-S mice, $n = 10$; F-D mice, $n = 10$).

One day after the injection of vehicle or Endo-N, mice were placed in a square chamber (18 × 18 × 40 cm) with a grid floor (0.2 cm diameter, spaced 0.6 cm apart; context A; Muromachi Kikai). The grid floor was connected to a shock generator scrambler (MFS-01; Muromachi Kikai). During the conditioning session, mice could move freely in the chamber for 2 min, and white noise was used as a conditioned stimulus (CS) for 30 s. During the last 2 s of CS presentation, a foot shock (0.5 mA, 2 s) was delivered as an unconditioned stimulus (US). The mice were subjected to two more CS–US pairings with 2-min intervals.

Eight days after the injection of vehicle or Endo-N, mice were placed in the conditioned chamber (context A) for 6 min as a contextual fear test. The next day, mice were placed in a triangular chamber (18 × 18 × 18 cm; context B; Muromachi Kikai) for 6 min as a cued fear test. Mice could move freely in the chamber, and the CS was applied during the last 3 min of the test period. The duration of the freezing behavior was measured using ANY-maze (Stoelting). Freezing was defined as a complete lack of motion for a minimum of 1 s.

On the second day of the fear conditioning test, mice were placed in an elevated plus-maze which consisted of two open arms (30 × 6 × 15 cm), two closed arms (30 × 6 cm), and a center platform (6 × 6 cm) (Muromachi Kikai). The apparatus was raised 40 cm above the floor. The center of the maze was illuminated at 100 lux. Mice were placed in an elevated plus-maze for 10 min and allowed to move freely in the field. The time spent in the open arm and the closed arm were automatically measured by ANY-maze (Stoelting). An entry was recorded when 50% of a mouse's body entered one of the arms. One day after the elevated plus-maze test, all mice were killed.

Western blot. A total of 24 mice were used for the Western blot: 12 mice treated with vehicle (NS mice, $n = 4$; R-S mice, $n = 4$; R-F mice, $n = 4$) and 12 mice treated with Endo-N (NS mice, $n = 4$; R-S mice, $n = 4$; R-F mice, $n = 4$). After overdosing with sodium pentobarbital (120 mg/kg, i.p.), deeply anesthetized animals were transcardially perfused with ice-cold PBS. Harvested brains were cut coronally on a vibrating microtome (VT1000S; Leica Microsystems) into 300 μm-thick sections in a bath of ice-cold PBS. The CA1 region of the hippocampus was dissected manually using a razor blade. Tissues were homogenized in PBS by pipetting. Protein concentrations were determined using the Rapid Protein Quantification Kit (Dojindo) and subjected to SDS-PAGE (ATTO). A Western blot was performed twice with comparable results, and a representative result was shown.

Transferred polyvinylidene difluoride membranes were blocked with 5.0% skim milk in PBS containing 0.1% Tween 20 (PBS-T) for 30 min at room temperature and incubated overnight at 4°C with the following antibodies: rabbit monoclonal anti-brain-derived neurotrophic factor (BDNF) antibody (1:10000; Abcam, RRID:AB_10862052), goat polyclonal anti-p11 (1:1500; R&D Systems), mouse monoclonal anti-PSA-NCAM (1:2000; AbCys SA), and mouse monoclonal anti-β-actin (1:30000; Sigma-Aldrich; RRID:AB_476692). The antibody against BDNF could recognize several BDNF isoforms, namely proBDNF (32 kDa and 42 kDa) and mature BDNF (14 kDa). After washing with PBS-T, membranes were incubated for 3 h at 20°C with the appropriate secondary antibodies: horseradish peroxidase (HRP)-conjugated rabbit anti-goat IgG (1:5000; Jackson ImmunoResearch), HRP-conjugated goat anti-rabbit IgG (1:5000; Jackson ImmunoResearch), or HRP-conjugated goat anti-mouse IgG (1:5000; Jackson ImmunoResearch). After washing with PBS-T, the bound antibodies were detected with Immobilon Western Chemiluminescent HRP Substrate (Millipore), and images were acquired using a luminoimage analyzer (ImageQuant LAS 4000mini; GE Healthcare). Equal-sized boxes were drawn around the bands, to measure band intensities, and the mean pixel values were measured using ImageJ 1.46.

Quantitative reverse transcription-polymerase chain reaction (qRT-PCR). In total, 24 mice were used for qRT-PCR: 12 mice treated with vehicle (NS mice, $n = 4$; R-S mice, $n = 4$; R-F mice, $n = 4$) and 12 mice treated with Endo-N (NS mice, $n = 4$; R-S mice, $n = 4$; R-F mice, $n = 4$). After overdosing with sodium pentobarbital (120 mg/kg, i.p.), deeply anesthetized animals were transcardially perfused with ice-cold PBS. Harvested brains were cut coronally on a vibrating microtome (VT1000S; Leica Microsystems) into 300 μm-thick sections in a bath of ice-cold PBS. The CA1 region of the hippocampus was dissected manually using a razor blade. We then isolated mRNA using the RNeasy plus mini kit, containing genomic DNA eliminator spin columns (QIAGEN). cDNA was synthesized from 500 ng of RNA in a 20 μl reaction volume using a first-strand cDNA synthesis kit (Roche Diagnostics) according to the manufacturer protocol. PCR was performed using the ABI7500 system (Applied Biosystems). The reaction mixture consisted of 10 μl of 2× Power SYBR Green PCR master mix (Applied Biosystems), 1 μl of cDNA, 2 μl of 5 μM forward and reverse primer mixture (Eurofins Genomics), and 7 μl of distilled water.

The following primer sequences were used for PCR: β-actin, 5′-CCTGAGCGCAAGTACTCTGTGT-3′ (forward) and 5′-GCTGATCCACATCTGCTGGAA-3′ (reverse); p11, 5′-CTT CAA AAT GCC ATC CCA AA-3′ (forward) and 5′-TAT TTT GTC CAC AGC CAG AGG-3′ (reverse); ST8Sia II, 5′-AGGCAGAGGTACAATCAGATCA-3′ (forward) and 5′-GAGAGAGCGTCTGGTTGTGTC-3′ (reverse); and ST8Sia IV, 5′-ATGCGCTCAATTAGAAAACGGT-3′ (forward) and 5′-CGATGAGTTGCGTCTCTTGGT-3′ (reverse).

Experimental design and statistical analyses. All experiments were designed considering a balance between the sample numbers to accurately perform statistical tests and the ethics guidelines for animal research. The numbers of animals, details of controls and experimental groups, and variables for the statistical analyses were described in the corresponding figure legends and tables. All datasets were analyzed with Origin 8.5 (OriginLab Corporation; RRID:SCR_014212) or SPSS 21 (IBM; RRID:

Table 1. Statistical summary of the Welch's *t* test

Figure no.	Variables	*t*-value	*p*-value
1C	Expression ratio of proCCK & [CCK]	$t_{5.11} = 4.838$	0.004
1D	Expression ratio of PSA-NCAM & [CCK]	$t_{3.18} = 3.618$	0.032
2B	Expression ratio of VIP & [VGluT3]	$t_{4.90} = 0.1893$	0.8574
2C	Density of VIP$^-$/[VGluT3$^+$] cells (so)	$t_{3.75} = 37.347$	<0.001
2C	Density of VIP$^-$/[VGluT3$^+$] cells (sp)	$t_{4.70} = 36.195$	<0.001
2C	Density of VIP$^-$/[VGluT3$^+$] cells (sr/slm)	$t_{3.72} = 23.282$	<0.001
2D	Proportion of VIP$^-$/[VGluT3$^+$] cells	$t_{6} = 86.422$	<0.001
2E	Density of VIP$^+$/[VGluT3$^-$] cells (so)	$t_{4.40} = 10.385$	<0.001
2E	Density of VIP$^+$/[VGluT3$^-$] cells (sp)	$t_{3.27} = 12.557$	<0.001
2E	Density of VIP$^+$/[VGluT3$^-$] cells (sr/slm)	$t_{3.01} = 14.345$	<0.001
2F	Proportion of VIP$^+$/[VGluT3$^-$] cells	$t_{6} = 65.001$	<0.001
2G	Density of VIP$^-$/[VGluT3$^-$] cells (so)	$t_{5.57} = 0.133$	0.899
2G	Density of VIP$^-$/[VGluT3$^-$] cells (sp)	$t_{5.87} = 1.444$	0.200
2G	Density of VIP$^-$/[VGluT3$^-$] cells (sr/slm)	$t_{3.27} = 2.561$	0.076
2H	Proportion of VIP$^-$/[VGluT3$^-$] cells	$t_{6} = 2.296$	0.061
3P	Expression ratio of VMAT2 & VGluT3	$t_{5.90} = 0.267$	0.799
4B	Expression ratio of $5HT_{3A}$ receptor	$t_{5.96} = 12.138$	<0.001
4D	Expression ratio of p11 & PSA-NCAM	$t_{4.77} = 2.167$	0.085
4F	Expression ratio of p11	$t_{5.40} = 24.586$	<0.001
5I	Intensity of PSA-NCAM (−1.46 mm)	$t_{5.97} = 6.094$	<0.001
5I	Intensity of PSA-NCAM (−1.94 mm)	$t_{4.52} = 7.822$	<0.001
5I	Intensity of PSA-NCAM (−2.54 mm)	$t_{5.99} = 2.942$	0.025
5J	Intensity of PSA-NCAM (−1.46 mm)	$t_{3.79} = 2.373$	0.082
5J	Intensity of PSA-NCAM (−1.94 mm)	$t_{5.95} = 11.972$	<0.001
5J	Intensity of PSA-NCAM (−2.54 mm)	$t_{5.96} = 1.930$	0.1027
6G	Proportion of VGluT3$^+$ lines	$t_{3.79} = 0.604$	0.580
6H	Proportion of VMAT2$^+$ lines	$t_{3.45} = 0.770$	0.491
6I	Density of Sox2$^+$/DCX$^-$/S100β^- neural stem cells	$t_{3.49} = 0.816$	0.466
6J	Density of Sox2$^-$/DCX$^+$/S100β^- neuronal progenitors	$t_{3.84} = 1.067$	0.348
6K	Density of Sox2$^+$/DCX$^-$/S100β^+ astrocytes	$t_{3.12} = 0.530$	0.631
10B	Freezing (trial 1)	$t_{34.32} = 1.343$	0.188
10B	Freezing (trial 2)	$t_{30.91} = 1.317$	0.198
10B	Freezing (trial 3)	$t_{37.87} = 1.322$	0.194

Table 2. Statistical summary of the one-way ANOVA

Figure no.	Variables	*F*-value	*p*-value
1E	Laminar distribution of [CCK$^+$] cells	$F_{2,9} = 9538.924$	<0.001
1F	Laminar distribution of PSA-NCAM$^+$ cells	$F_{2,9} = 1832.223$	<0.001
2I	Proportion of PSA-NCAM$^+$ cells	$F_{2,9} = 9133.892$	<0.001
2J	Proportion of PSA-NCAM$^-$ cells	$F_{2,9} = 310.177$	<0.001
3Q	Proportion of VGluT1$^+$ lines	$F_{2,9} = 0.536$	0.602
3R	Proportion of GAD$^+$ lines	$F_{2,9} = 0.311$	0.741
3S	Proportion of VGluT3$^+$ lines	$F_{2,9} = 37.041$	<0.001
3T	Proportion of VMAT2$^+$ lines	$F_{2,9} = 43.912$	<0.001
8E	Intensity of PSA-NCAM	$F_{2,12} = 96.902$	<0.001
8F	Density of PSA-NCAM$^+$ cells	$F_{2,9} = 1.434$	0.288
8G	Density of [VGluT3$^+$]/[CCK$^+$] cells (vehicle)	$F_{2,9} = 2.047$	0.185
8H	Density of [VGluT3$^+$]/[CCK$^+$] cells (Endo-N)	$F_{2,9} = 1.176$	0.352
8J	Expression of PSA-NCAM (WB)	$F_{2,8} = 6.322$	0.033
8K	Expression of ST8Sia II (qRT-PCR)	$F_{2,9} = 2.987$	0.101
8L	Expression of ST8Sia IV (qRT-PCR)	$F_{2,9} = 13.997$	0.002

SCR_002865). Welch's *t* test (Table 1), one-way analysis of variance (ANOVA) with *post hoc* Tukey's honestly significant difference (HSD) test (Table 2), and two-way ANOVA with *post hoc* Tukey's HSD test (Table 3) were performed in this study. Results were expressed and plotted as mean ± SD. Differences were considered significant when $p < 0.05$.

Results

Colocalization of CCK mRNA, proCCK, and PSA-NCAM

CCK peptides are derived from proCCK and have a bioactive sequence at the C terminus (Rehfeld et al., 2007). To understand the relationship between PSA-NCAM and CCK$^+$ cells in the CA1 region of the mouse hippocampus, we examined the patterns of colocalization of CCK mRNA, proCCK, and PSA-NCAM. Combined FISH and immunohistochemistry showed that CCK mRNA and proCCK were colocalized with each other (Fig. 1*A*), and CCK mRNA and PSA-NCAM were also frequently colocalized with each other (Fig. 1*B*).

We next quantitatively estimated the colocalization of CCK mRNA, proCCK, and PSA-NCAM (Fig. 1*C–F*, Tables 1, 2). The optical disector analysis showed that 76.1% of CCK mRNA$^+$ cells were immunoreactive for proCCK, whereas 93.0% of proCCK$^+$ cells expressed CCK mRNA (Fig. 1*C*). Thus, we considered that the major population of CCK$^+$ cells might be labeled by CCK mRNA or proCCK.

Our analysis also showed that 65.5% of CCK mRNA$^+$ cells were colocalized with PSA-NCAM, whereas 88.6% of PSA-NCAM$^+$ cells expressed CCK mRNA (Fig. 1*D*). The laminar distribution analysis showed that both CCK mRNA$^+$ cells and PSA-NCAM$^+$ cells were distributed in the strata radiatum and lacunosum moleculare, and only a few were located in the strata oriens and pyramidale (Fig. 1*E*,*F*). Together, these results show that CCK is expressed in the vast majority of PSA-NCAM$^+$ cells, whereas PSA-NCAM represents a substantial population of CCK$^+$ cells.

Subtype-specific colocalization of CCK$^+$ cells with PSA-NCAM

It has been suggested that CCK$^+$ cells in the CA1 region of the hippocampus may be divided into three subtypes: VIP$^+$/VGluT3$^+$ cells, VIP$^-$/VGluT3$^+$ cells, and VIP$^-$/VGluT3$^-$ cells (Somogyi et al., 2004). We thus aimed to know whether PSA-NCAM might be associated with a specific subtype of CCK$^+$ cells by using combined FISH and immunohistochemistry (Fig. 2*A*). We first confirmed that the expression ratio (%) of VIP in VGluT3$^+$/CCK$^+$ cells, was ~2% and that of VGluT3 in VIP$^+$/CCK$^+$ cells was ~5% (Fig. 2*B*, Table 1). These results support that expressions of VGluT3 and VIP in CCK$^+$ cells are mutually exclusive.

We next examined the colocalization of PSA-NCAM and three subtypes of CCK$^+$ cells defined by VIP and VGluT3: VIP$^-$/VGluT3$^+$ cells, VIP$^+$/VGluT3$^-$ cells, and VIP$^-$/VGluT3$^-$ cells (Fig. 2*C–J*, Tables 1, 2). The densities (×1000/mm^3) of VIP$^-$/VGluT3$^+$/CCK$^+$ cells colocalized with PSA-NCAM were significantly higher than those lacking PSA-NCAM in all layers of the CA1 region (Fig. 2*C*). In the total area of the CA1 region, 93.6% of VIP$^-$/VGluT3$^+$/CCK$^+$ cells were colocalized with PSA-NCAM (Fig. 2*D*). The densities (×1000/mm^3) of VIP$^+$/VGluT3$^-$/CCK$^+$ cells colocalized with PSA-NCAM were significantly lower than those lacking PSA-NCAM in all layers of the CA1 region (Fig. 2*E*). In the total area of the CA1 region, 92.2% of VIP$^+$/VGluT3$^-$/CCK$^+$ cells lacked PSA-NCAM (Fig. 2*F*). The densities (×1000/mm^3) of VIP$^-$/VGluT3$^-$/CCK$^+$ cells were low in all layers of the CA1 region (Fig. 2*G*). The proportions (%) of VIP$^-$/VGluT3$^-$/CCK$^+$ cells colocalized with PSA-NCAM were comparable to those lacking PSA-NCAM in the total area of the CA1 region (Fig. 2*H*).

We then compared the subtype compositions of PSA-NCAM$^+$/CCK$^+$ cells and PSA-NCAM$^-$/CCK$^+$ cells. As expected, VIP$^-$/VGluT3$^+$ cells represented 88.6% of PSA-NCAM$^+$/CCK$^+$ cells (Fig. 2*I*), and VIP$^+$/VGluT3$^-$ cells accounted for 73.1% of PSA-NCAM$^-$/CCK$^+$ cells (Fig. 2*J*). These findings indicate that PSA-NCAM may be a specific marker of VGluT3$^+$/CCK$^+$ cells.

Table 3. Statistical summary of the two-way ANOVA

		Endo-N		Stress and/or FLX		Endo-N × (stress and/or FLX)	
Figure no.	Variables	*F*-value	*p*-value	*F*-value	*p*-value	*F*-value	*p*-value
7B	Distance traveled in OFT	$F_{1,54} = 0.221$	0.64	$F_{2,54} = 3.107$	0.053	$F_{2,54} = 1.917$	0.157
7C	Outer/total time ratio	$F_{1,54} = 0.051$	0.822	$F_{2,54} = 3.094$	0.054	$F_{2,54} = 0.785$	0.461
7D	Center zone entry	$F_{1,54} = 0.277$	0.601	$F_{2,54} = 0.876$	0.422	$F_{2,54} = 0.104$	0.901
7E	Distance traveled in FST	$F_{1,54} = 8.032$	0.006	$F_{2,54} = 21.714$	<0.001	$F_{2,54} = 13.209$	<0.001
7F	Immobility time	$F_{1,54} = 7.281$	0.01	$F_{2,54} = 68.158$	<0.001	$F_{2,54} = 13.486$	<0.001
9E	Intensity of p11 (total GAD$^+$ cells)	$F_{1,12} = 12.787$	0.004	$F_{2,12} = 8.107$	0.006	$F_{2,12} = 7.626$	0.007
9F	Intensity of p11 (CCK$^+$/GAD$^+$ cells)	$F_{1,12} = 18.856$	0.001	$F_{2,12} = 10.011$	0.003	$F_{2,12} = 5.657$	0.019
9G	Intensity of p11 (CCK$^-$/GAD$^+$ cells)	$F_{1,12} = 2.218$	0.162	$F_{2,12} = 0.275$	0.764	$F_{2,12} = 0.499$	0.619
9I	Expression of p11 (WB)	$F_{1,18} = 29.077$	<0.001	$F_{2,18} = 24.342$	<0.001	$F_{2,18} = 12.459$	0.001
9J	Expression of p11 (qRT-PCR)	$F_{1,18} = 11.095$	0.004	$F_{2,18} = 24.947$	<0.001	$F_{2,18} = 5.115$	0.017
9L	Expression of proBDNF (WB)	$F_{1,18} = 0.078$	0.784	$F_{2,18} = 3.418$	0.067	$F_{2,18} = 0.702$	0.515
9M	Expression of mature BDNF (WB)	$F_{1,18} = 0.001$	0.98	$F_{2,18} = 15.538$	<0.001	$F_{2,18} = 1.585$	0.245
		Endo-N		DZP		Endo-N × DZP	
		F-value	*p*-value	*F*-value	*p*-value	*F*-value	*p*-value
10C	Contextual fear (context A)	$F_{1,36} = 3.524$	0.069	$F_{1,36} = 17.430$	<0.001	$F_{1,36} = 0.243$	0.625
10D	Contextual fear (context B)	$F_{1,36} = 0.010$	0.919	$F_{1,36} = 1.950$	0.171	$F_{1,36} = 0.099$	0.755
10E	Cued fear	$F_{1,36} = 0.001$	0.997	$F_{1,36} = 22.506$	<0.001	$F_{1,36} = 0.003$	0.960
10F	Time spent in open arm	$F_{1,36} = 0.003$	0.954	$F_{1,36} = 24.006$	<0.001	$F_{1,36} = 2.791$	0.103
10G	Number of open arm entry	$F_{1,36} = 0.923$	0.343	$F_{1,36} = 31.178$	<0.001	$F_{1,36} = 0.923$	0.343

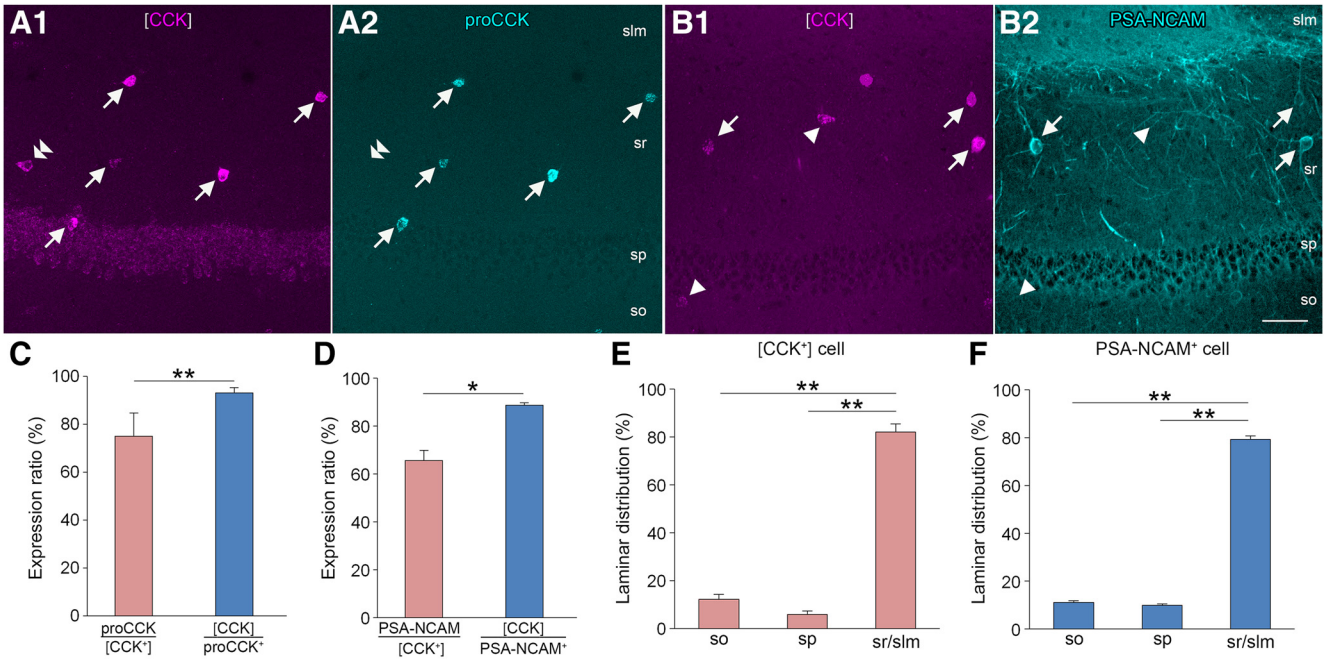

Figure 1. Colocalization of CCK mRNA, proCCK, and PSA-NCAM in the CA1 region. ***A***, Double fluorescence for CCK mRNA (magenta, ***A1***) and proCCK (cyan, ***A2***). Markers enclosed in brackets denote mRNAs detected by FISH. Arrows represent proCCK$^+$/CCK mRNA$^+$ cells, and double arrowheads represent proCCK$^-$/CCK mRNA$^+$ cells. ***B***, Double fluorescence for CCK mRNA (magenta, ***B1***) and PSA-NCAM (cyan, ***B2***). Arrows represent PSA-NCAM$^+$/CCK mRNA$^+$ cells, and arrowheads represent PSA-NCAM$^-$/CCK mRNA$^+$ cells. ***C***, The expression ratio (%) of proCCK in CCK mRNA$^+$ cells and that of CCK mRNA in proCCK$^+$ cells. ***D***, The expression ratio (%) of PSA-NCAM around CCK mRNA$^+$ cells and that of CCK mRNA in PSA-NCAM$^+$ cells. ***E***, ***F***, The laminar distributions (%) of CCK mRNA$^+$ cells (***E***) and PSA-NCAM$^+$ cells (***F***) in the CA1 region. Data are presented as mean ± SD ($n = 4$ mice per group). Statistical significance is represented with asterisks: *$p < 0.05$; **$p < 0.01$. slm, stratum lacunosum-moleculare; so, stratum oriens; sp, stratum pyramidale; sr, stratum radiatum. Scale bar in ***B2***, 50 μm (applies to ***A*** and ***B***).

We examined the potential colocalization of PSA-NCAM with VGluT3$^+$/CCK$^+$ boutons in the stratum pyramidale of the CA1 region. In this experiment, we identified CCK$^+$ synaptic boutons using the anti-CCK antibody kindly provided by the CURE/Gastroenteric Biology Center. Because both the anti-CCK and anti-PSA-NCAM antibodies were raised in mice, we performed double staining for CCK and VGluT3 (Fig. 2*K*) and PSA-NCAM and VGluT3 (Fig. 2*L*) and found several VGluT3$^+$/CCK$^+$ boutons and VGluT3$^+$/PSA-NCAM$^+$ boutons in the stratum pyramidale of the CA1 region. These results suggest that the synaptic terminals of VGluT3$^+$/CCK$^+$ cells may be colocalized with PSA-NCAM.

Subtype-specific difference in the synaptic terminals onto CCK$^+$ cells

It has been shown that VGluT3$^+$/CCK$^+$ cells are heavily targeted by VGluT3$^+$ serotonergic terminals (Somogyi et al., 2004). We thus aimed to clarify the potential subtype-specific differences in the synaptic boutons terminating onto CCK$^+$ cells (Fig. 3). In

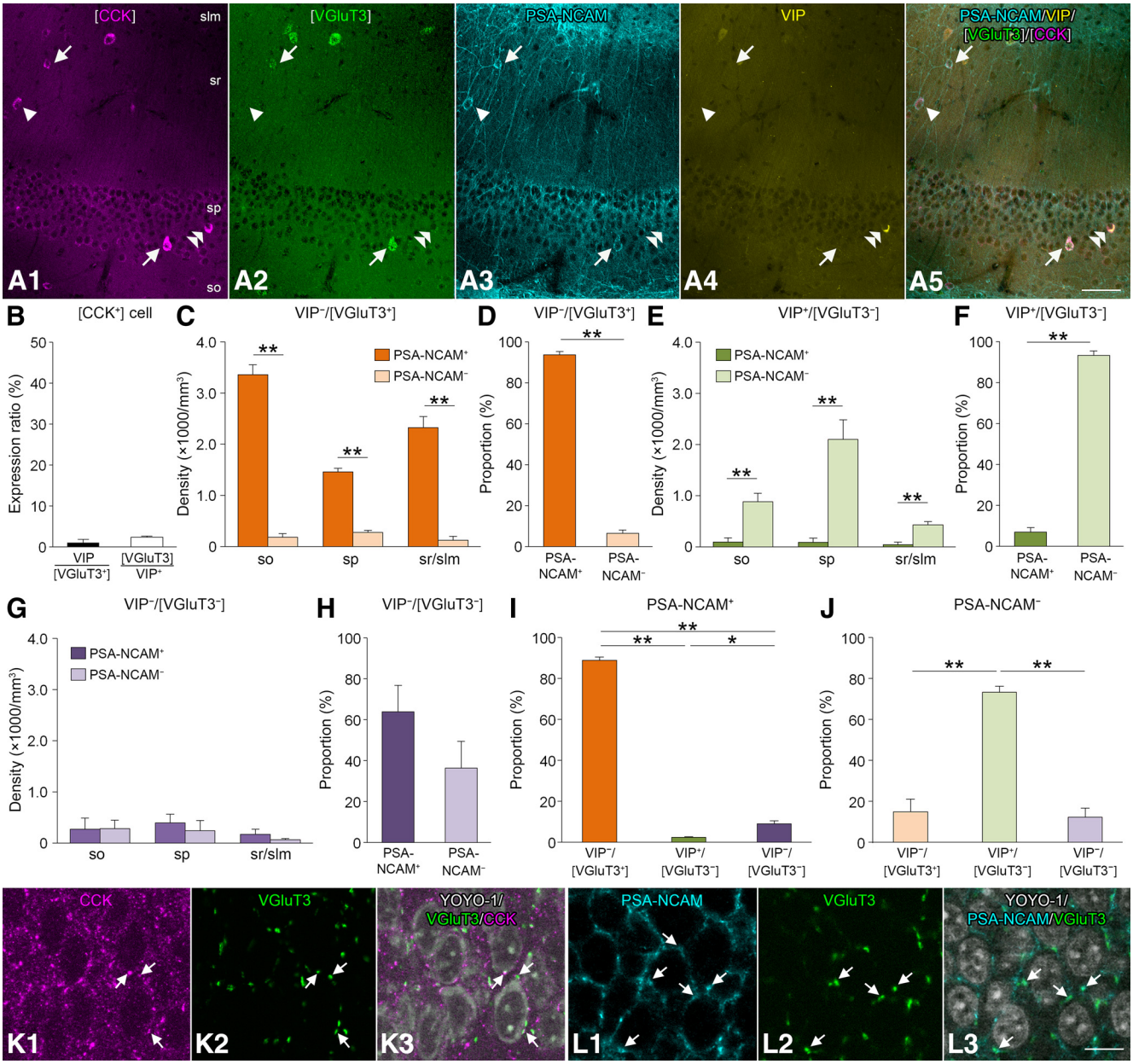

Figure 2. Subtype-specific colocalization of CCK$^+$ cells with PSA-NCAM in the CA1 region. ***A***, Quadruple fluorescence for CCK mRNA (magenta, ***A1***), VGluT3 mRNA (green, ***A2***), PSA-NCAM (cyan, ***A3***), VIP (yellow, ***A4***), and merged (***A5***). Markers enclosed in brackets denote mRNAs detected by FISH. Arrows represent PSA-NCAM$^+$/VIP$^-$/VGluT3$^+$/CCK$^+$ cells, arrowheads represent PSA-NCAM$^+$/VIP$^-$/VGluT3$^-$/CCK$^+$ cells, and double arrowheads represent PSA-NCAM$^-$/VIP$^+$/VGluT3$^-$/CCK$^+$ cells. ***B***, The expression ratio (%) of VIP in VGluT3$^+$/CCK$^+$ cells and that of VGluT3 in VIP$^+$/CCK$^+$ cells. ***C***, The densities (×1000/mm^3) of VIP$^-$/VGluT3$^+$/CCK$^+$ cells colocalized with or without PSA-NCAM. ***D***, The proportions (%) of VIP$^-$/VGluT3$^+$/CCK$^+$ cells colocalized with or without PSA-NCAM. ***E***, The densities (×1000/mm^3) of VIP$^+$/VGluT3$^-$/CCK$^+$ cells. ***F***, The proportions (%) of VIP$^+$/VGluT3$^-$/CCK$^+$ cells colocalized with or without PSA-NCAM. ***G***, The densities (×1000/mm^3) of VIP$^-$/VGluT3$^-$/CCK$^+$ cells. ***H***, The proportions (%) of VIP$^-$/VGluT3$^-$/CCK$^+$ cells colocalized with or without PSA-NCAM. ***I***, ***J***, The proportions (%) of three subtypes of CCK$^+$ cells colocalized with (***I***) or without (***J***) PSA-NCAM. ***K***, Triple fluorescence for CCK (magenta, ***K1***), VGluT3 (green, ***K2***), and YOYO-1 (gray, ***K3***) in the pyramidal cell layer of the CA1 region. Arrows represent VGluT3$^+$/CCK$^+$ synaptic boutons. ***L***, Triple fluorescence for PSA-NCAM (cyan, ***L1***), VGluT3 (green, ***L2***), and YOYO-1 (gray, ***L3***) in the pyramidal cell layer of the CA1 region. Arrows represent PSA-NCAM$^+$/VGluT3$^+$ synaptic boutons. Data are presented as mean ± SD ($n = 4$ mice per group). Statistical significance is represented with asterisks: *$p < 0.05$; **$p < 0.01$. slm, stratum lacunosum-moleculare; so, stratum oriens; sp, stratum pyramidale; sr, stratum radiatum. Scale bars: ***A5***, 50 μm (applies to ***A***); ***L3***, 10 μm (applies to ***K*** and ***L***).

this experiment, a combined FISH and DIC imaging allowed us to identify the outlines of the somata of the CCK$^+$ cells (Fig. 3*A*).

We first examined the potential colocalization of VMAT2 and VGluT3 in synaptic boutons terminating on CCK$^+$ cells, because it has been reported that expression of VGluT3 in VMAT2$^+$ synaptic terminals actively accelerates serotonergic neurotransmission (Amilhon et al., 2010). Combined FISH and immunohistochemistry showed that the immunoreactivities for VMAT2 and VGluT3 around the somata of CCK$^+$ cells were well colocalized with each other (Fig. 3*B*). We performed the line profile analysis (Yamada et al., 2011), to quantitatively evaluate the colocalization of VMAT2 and VGluT3 in serotonergic boutons onto CCK$^+$ cells. The line profile analysis is suitable for the structural examination of fluorescence images at the synaptic level (Wong et al., 2018). Lines, perpendicular to somata, were drawn around the entire circumferential surface of the CCK$^+$ cells at 2-μm intervals (Fig. 3*B*), and the pixel intensities were measured (Fig. 3*C*). The line profile analysis showed that 74.7% of

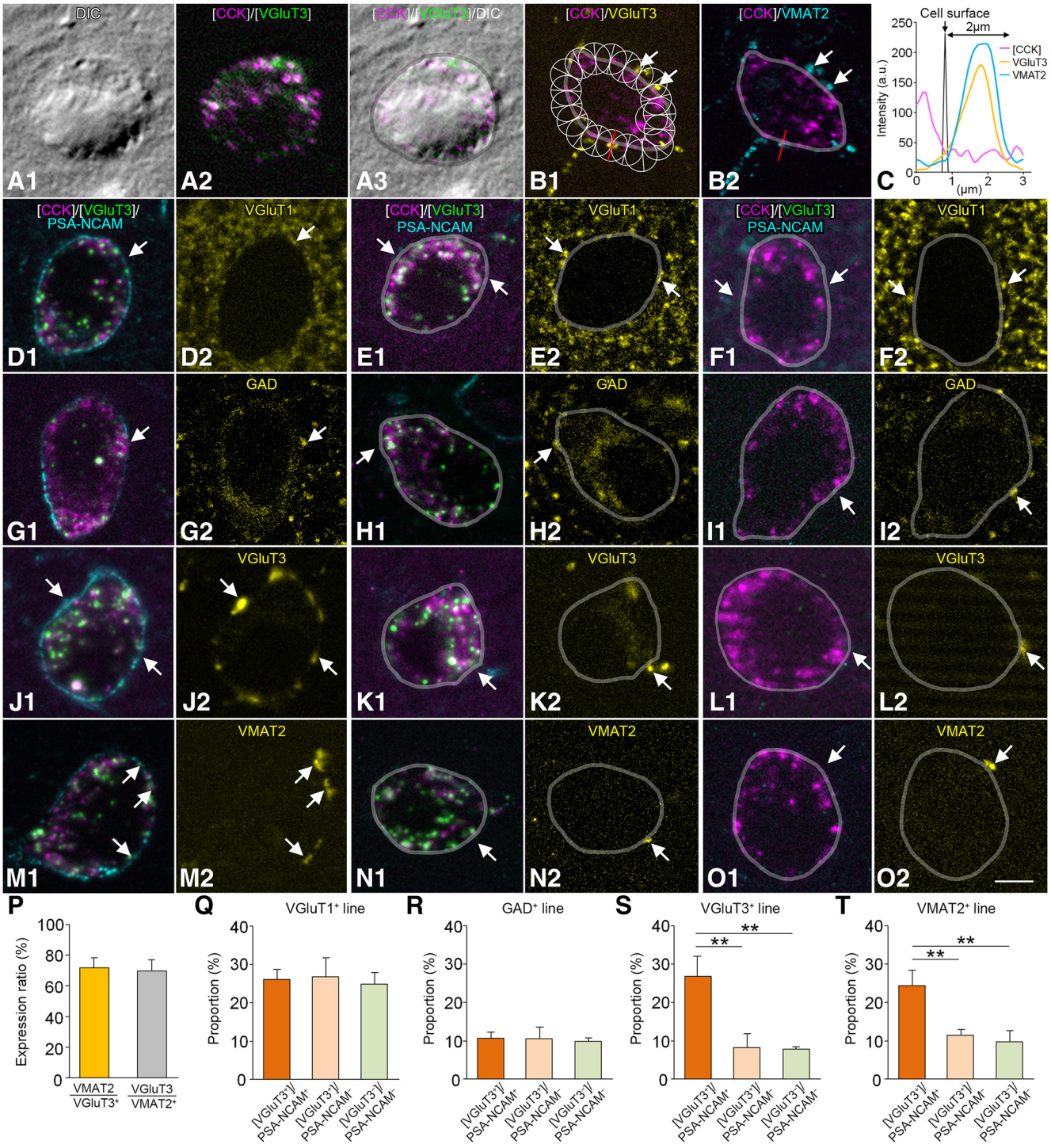

Figure 3. Subtype-specific differences in the synaptic boutons contacting CCK $^{+}$ cells in the CA1 region. ***A***, DIC image (***A1***) is combined with fluorescence for CCK mRNA (magenta, ***A2***) to identify the outline of soma (gray line, ***A3***). Markers enclosed in brackets denote mRNAs detected by FISH. ***B***, Triple fluorescence for CCK mRNA (magenta, ***B1***,***2***), VGluT3 (yellow, ***B1***), and VMAT2 (gray, ***B2***). Arrows represent VMAT2 $^{+}$/VGluT3 $^{+}$ synaptic boutons contacting the soma. ***C***, Representative plot of the gray level values of CCK mRNA (magenta), VGluT3 (yellow), and VMAT2 (cyan) along the red line in ***B1***,***2***. The line profile is defined by order of peaks of CCK mRNA, VGluT3, and VMAT2 within 2 μm from the cell surface defined by the DIC image. ***D–F***, Quadruple fluorescence for PSA-NCAM (cyan, ***D1***, ***E1***, ***F1***), VGluT3 mRNA (green, ***D1***, ***E1***, ***F1***), CCK mRNA (magenta, ***D1***, ***E1***, ***F1***), and VGluT1 (yellow, ***D2***, ***E2***, ***F2***). Arrows represent VGluT1 $^{+}$ boutons contacting the soma. ***G–I***, Quadruple fluorescence for PSA-NCAM (cyan, ***G1***, ***H1***, ***I1***), VGluT3 mRNA (green, ***G1***, ***H1***, ***I1***), CCK mRNA (magenta, ***G1***, ***H1***, ***I1***), and GAD (yellow, ***G2***, ***H2***, ***I2***). Arrows represent GAD $^{+}$ boutons contacting the soma. ***J–L***, Quadruple fluorescence for PSA-NCAM (cyan, ***J1***, ***K1***, ***L1***), VGluT3 mRNA (green, ***J1***, ***K1***, ***L1***), CCK mRNA (magenta, ***J1***, ***K1***, ***L1***), and VGluT3 (yellow, ***J2***, ***K2***, ***L2***). Arrows represent VGluT3 $^{+}$ serotonergic boutons contacting the soma. ***M–O***, Quadruple fluorescence for PSA-NCAM (cyan, ***M1***, ***N1***, ***O1***), VGluT3 mRNA (green, ***M1***, ***N1***, ***O1***), CCK mRNA (magenta, ***M1***, ***N1***, ***O1***), and VGluT3 (yellow, ***M2***, ***N2***, ***O2***). Arrows represent VMAT2 $^{+}$ serotonergic boutons contacting the soma. ***P***, The expression ratio (%) of VMAT2 in the total VGluT3 $^{+}$ lines and that of VGluT3 in the total VMAT2 $^{+}$ lines around the somata of CCK $^{+}$ cells. ***Q–T***, The proportions (%) of VGluT1 $^{+}$ (***Q***), GAD $^{+}$ (***R***), VGluT3 $^{+}$ (***S***), and VMAT2 $^{+}$ (***T***) lines around the somata of CCK $^{+}$ cells divided into three subtypes. Data are presented as mean $\pm$ SD ($n = 4$ mice per group). Statistical significance is represented with asterisks: $^{**}p < 0.01$. Scale bar: ***O2***, 3 μm (applies to ***A***, ***B***, and ***D–O***).

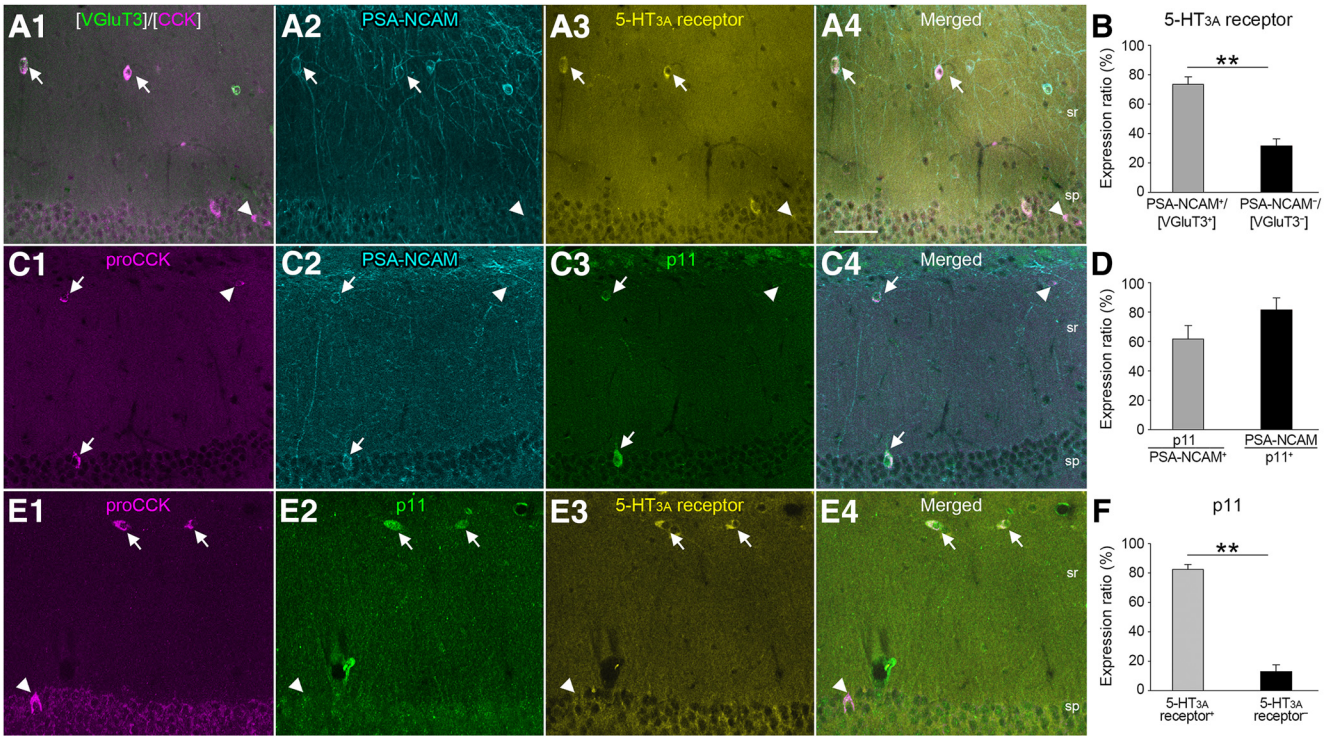

Figure 4. Colocalization of 5-HT$_{3A}$ receptor, CCK, and p11 in the CA1 region. ***A***, Quadruple fluorescence for VGluT3 mRNA (green, ***A1***), CCK mRNA (magenta, ***A1***), PSA-NCAM (cyan, ***A2***), 5-HT$_{3A}$ receptor (yellow, ***A3***), and merged (***A4***). Markers enclosed in brackets denote mRNAs detected by FISH. Arrows represent 5-HT$_{3A}$ receptor$^+$/PSA-NCAM$^+$/VGluT3$^+$/CCK$^+$ cells, and arrowheads represent 5-HT$_{3A}$ receptor$^-$/PSA-NCAM$^-$/VGluT3$^-$/CCK$^+$ cells. ***B***, The expression ratios (%) of 5-HT$_{3A}$ receptors in PSA-NCAM$^+$/VGluT3$^+$/CCK$^+$ cells and PSA-NCAM$^-$/VGluT3$^-$/CCK$^+$ cells. ***C***, Triple fluorescence for proCCK (magenta, ***C1***), PSA-NCAM (cyan, ***C2***), p11 (green, ***C3***), and merged (***C4***). Arrows represent p11$^+$/PSA-NCAM$^+$/proCCK$^+$ cells, and arrowheads represent p11$^-$/PSA-NCAM$^+$/proCCK$^+$ cells. ***D***, The expression ratio (%) of p11 in PSA-NCAM$^+$/proCCK$^+$ cells and that of PSA-NCAM in p11$^+$/proCCK$^+$ cells. ***E***, Triple fluorescence for proCCK (magenta, ***E1***), p11 (green, ***E2***), 5-HT$_{3A}$ receptor (yellow, ***E3***), and merged (***E4***). Arrows represent p11$^+$/5-HT$_{3A}$ receptor$^+$/proCCK$^+$ cells and arrowheads represent p11$^-$/5-HT$_{3A}$ receptor$^-$/proCCK$^+$ cells. ***F***, The expression ratios (%) of p11 in 5-HT$_{3A}$ receptor$^+$/proCCK$^+$ cells and 5-HT$_{3A}$ receptor$^-$/proCCK$^+$ cells. Data are presented as mean ± SD ($n = 4$ mice per group). Statistical significance is represented with asterisks: $^{**}p < 0.01$. sp, stratum pyramidale; sr, stratum radiatum. Scale bar in ***A4***, 50 μm (applies to ***A***, ***C***, and ***E***).

VGluT3$^+$ lines expressed VMAT2, and 73.2% of VMAT2$^+$ lines expressed VGluT3 (Fig. 3*P*), which suggests that CCK$^+$ cells may be involved in serotonergic neurotransmission via VMAT2$^+$/VGluT3$^+$ synaptic terminals.

According to the molecular profile of the path crossing the synaptic environment, we defined three types of lines: VMAT2$^+$/VGluT3$^-$ line, the profile making contact with the soma of CCK$^+$ cell is a VMAT2$^+$/VGluT3$^-$ bouton; VMAT2$^-$/VGluT3$^+$ line, the profile making contact with the soma of CCK$^+$ cell is a VMAT2$^-$/VGluT3$^+$ bouton; VMAT2$^+$/VGluT3$^+$ line, the profile making contact with the soma of CCK$^+$ cell is a VMAT2$^+$/VGluT3$^+$ bouton.

To examine the subtype-specific difference in synaptic boutons making contact with CCK$^+$ cells, we divided CCK$^+$ cells into three groups according to the expression of PSA-NCAM and VGluT3: PSA-NCAM$^+$/VGluT3$^+$ cells (Fig. 3*D*,*G*,*J*,*M*), PSA-NCAM$^-$/VGluT3$^+$ cells (Fig. 3*E*,*H*,*K*,*N*), and PSA-NCAM$^-$/VGluT3$^-$ cells (Fig. 3*F*,*I*,*L*,*O*). Dense VGluT1$^+$ boutons (Fig. 3*D–F*) and few GAD$^+$ boutons (Fig. 3*G–I*) were seen nearby three groups of CCK$^+$ cells. VGluT3$^+$ serotonergic boutons and VMAT2$^+$ serotonergic boutons were scattered nearby the PSA-NCAM$^+$/VGluT3$^+$ cells (Fig. 3*J*,*M*), whereas they were relatively few near the PSA-NCAM$^-$/VGluT3$^+$ cells (Fig. 3*K*,*N*) and the PSA-NCAM$^-$/VGluT3$^-$ cells (Fig. 3*L*,*O*).

We defined VGluT1$^+$, GAD$^+$, VGluT3$^+$, and VMAT2$^+$ lines, as above, to quantitatively estimate the synaptic boutons terminating onto CCK$^+$ cells. The results of the line profile analysis showed that the proportions (%) of VGluT1$^+$ lines (≈25%) and GAD$^+$ lines (≈10%) were comparable among the three subtypes of CCK$^+$ cells (Fig. 3*Q*,*R*, Table 2). By contrast, the proportions of VGluT3$^+$ lines and VMAT2$^+$ lines in the CCK$^+$ cells were significantly higher in PSA-NCAM$^+$/VGluT3$^+$ cells (26.7% of VGluT3$^+$ lines; 24.3% of VMAT2$^+$ lines) than in PSA-NCAM$^-$/VGluT3$^+$ cells (8.2% of VGluT3$^+$ lines; 11.4% of VMAT2$^+$ lines) and in PSA-NCAM$^-$/VGluT3$^-$ cells (7.8% of VGluT3$^+$ lines; 9.7% of VMAT2$^+$ lines) (Fig. 3*S*,*T*, Table 2); thus, suggesting that serotonergic terminals may highly innervate VGluT3$^+$/CCK$^+$ cells colocalized with PSA-NCAM than other CCK$^+$ cells that lack PSA-NCAM, whereas there may be no subtype-specific differences in the glutamatergic and GABAergic terminals onto CCK$^+$ cells.

Subtype-specific difference in the expression of 5-HT$_{3A}$ receptors and p11 in CCK$^+$ cells

Earlier research showed that serotonin release might be nonsynaptic, and inputs are not limited to cell bodies (Umbriaco et al., 1995). We thus examined the potential subtype-specific differences in expression of 5-HT$_{3A}$ receptors in CCK$^+$ cells. Although 5-HT$_{3A}$ receptors were observed in both PSA-NCAM$^+$/VGluT3$^+$/CCK$^+$ cells and PSA-NCAM$^-$/VGluT3$^-$/CCK$^+$ cells (Fig. 4*A*), the expression ratio of 5-HT$_{3A}$ receptors in the PSA-NCAM$^+$/VGluT3$^+$/CCK$^+$ cells (73.5%) was higher than that in the PSA-NCAM$^-$/VGluT3$^-$/CCK$^+$ cells (31.7%) (Fig. 4*B*, Table 1), which indicates that 5-HT$_{3A}$ receptors may be more closely associated with VGluT3$^+$/CCK$^+$ cells colocalized with PSA-NCAM compared with VGluT3$^-$/CCK$^+$ cells that lack PSA-NCAM.

To untangle the potential involvement of PSA-NCAM in serotonergic signaling within CCK$^+$ cells, we examined the patterns of expression of p11, an adaptor protein of 5-HT receptors (Zhang et al., 2008). Triple fluorescence for proCCK, PSA-NCAM, and p11 demonstrated that p11 was frequently expressed in PSA-NCAM$^+$/proCCK$^+$ cells in the CA1 region (Fig. 4*C*). The expression ratio (%) of p11 in PSA-NCAM$^+$/proCCK$^+$ cells (61.7%) was comparable to that of PSA-NCAM in p11$^+$/proCCK$^+$ cells (81.5%) (Fig. 4*D*, Table 1). These results indicate that p11 and PSA-NCAM may be strongly associated with each other in CCK$^+$ cells.

While p11 was demonstrated as important in the regulation of 5-HT$_{1B}$ receptors (Svenningsson et al., 2006), several studies have reported that serotonergic inputs onto CCK$^+$ cells may be mediated by 5-HT$_{3A}$ receptors (Morales and Bloom, 1997; Yoshida et al., 2019). To address this issue, we examined the colocalization of p11 and 5-HT$_{3A}$ receptors in proCCK$^+$ cells in the CA1 region (Fig. 4*E*). In general, p11 was seen in 5-HT$_{3A}$ receptor$^+$/proCCK$^+$ cells. The expression ratio (%) of p11 was higher in HT$_{3A}$ receptor$^+$/proCCK$^+$ cells (82.4%) than in that of 5-HT$_{3A}$ receptor$^-$/proCCK$^+$ cells (13.5%) (Fig. 4*F*, Table 1). These findings suggest that p11 may be involved in signaling via 5-HT$_{3A}$ receptors in CCK$^+$ cells.

Digestion of PSA-NCAM in the CA1 region by local Endo-N injection

Endo-N was injected into four sites of the CA1 region bilaterally (eight sites in total) (Fig. 5*A*,*B*), to further understand the functional significance of PSA-NCAM. The extent the digestion of PSA-NCAM is shown in the hippocampal sections at bregma –1.46 mm (Fig. 5*C*,*D*), –1.94 mm (Fig. 5*E*,*F*), and –2.54 mm (Fig. 5*G*,*H*). The immunoreactivity for PSA-NCAM was lower in Endo-N treated mice than in vehicle-treated mice.

Using the hippocampal sections at the bregma levels mentioned above, we measured the immunoreactivity for PSA-NCAM in the CA1 region and dentate gyrus. The fluorescence intensities for PSA-NCAM in the CA1 region were significantly lower in Endo-N-treated mice than in vehicle-treated mice at all bregma levels (Fig. 5*I*, Table 1). In contrast, the fluorescence intensities for PSA-NCAM in the dentate gyrus were comparable between Endo-N-treated mice and vehicle-treated mice at bregma –1.46 mm and –2.54 mm, whereas they were lower in Endo-N-treated mice compared with

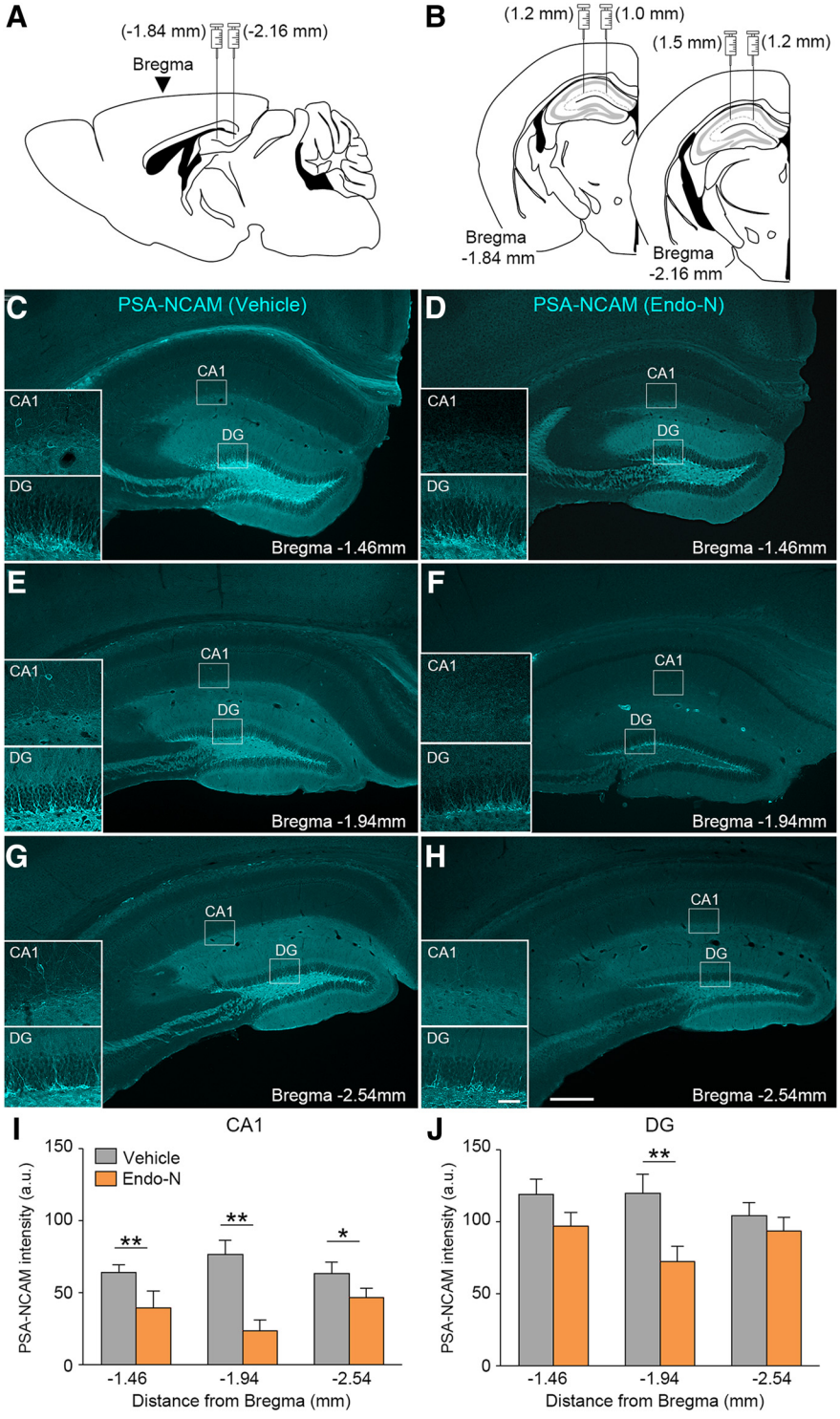

Figure 5. Extent of digestion of PSA-NCAM by local injection of Endo-N into the CA1 region. ***A***, ***B***, Schematic illustrations of the hippocampal injection sites in sagittal (***A***) and coronal planes (***B***). Values in parenthesis in (***A***) represent the anteroposterior coordinates relative to the bregma, and those in parenthesis in (***B***) represent the lateral coordinates relative to the midline. ***C–H***, Representative fluorescence for PSA-NCAM in the hippocampus of mice that received a local injection of vehicle (***C***, ***E***, ***G***) or Endo-N (***D***, ***F***, ***H***) into the CA1 region. The anteroposterior positions of the sections from the bregma were –1.46 mm (***C***, ***D***), –1.94 mm (***E***, ***F***), and –2.54 mm (***G***, ***H***). Insets show the magnified images highlighted by rectangles in the CA1 region (CA1) and dentate gyrus (DG). ***I***, ***J***, The fluorescence intensities (arbitrary unit, a.u.) of PSA-NCAM in the CA1 region (***I***) and dentate gyrus (***J***). Data are presented as mean ± SD ($n = 4$ mice per group). Statistical significance is represented with asterisks: *$p < 0.05$; **$p < 0.01$. Scale bars: ***H***, 200 μm (applies to ***C–H***); inset of ***H***, 20 μm (applies to insets of ***C–H***).

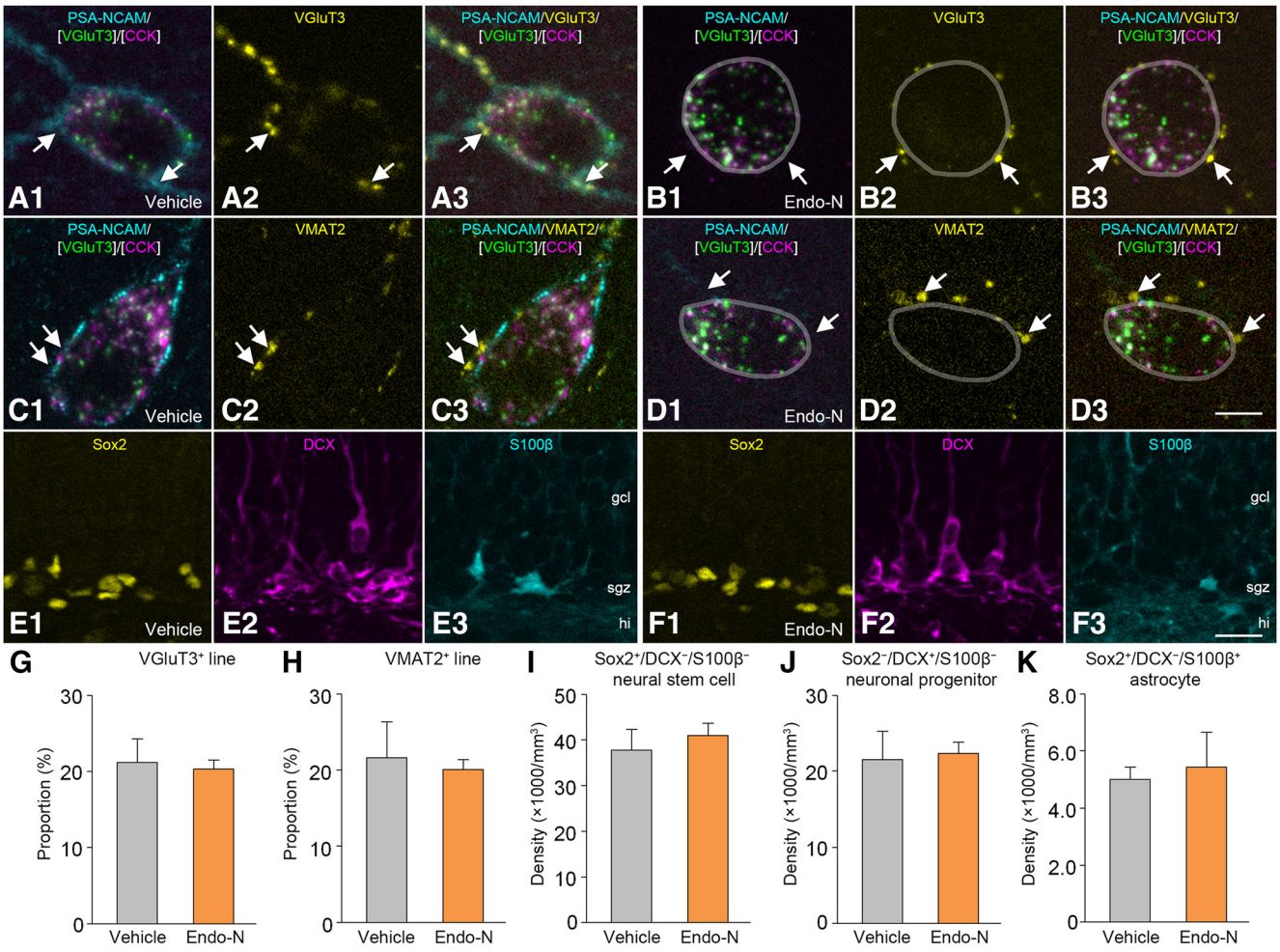

Figure 6. Digestion of PSA-NCAM in the CA1 region affects neither the serotonergic terminals nor the adult hippocampal neurogenesis. ***A***, ***B***, Quadruple fluorescence for PSA-NCAM (cyan, ***A1***, ***B1***), VGluT3 mRNA (green, ***A1***, ***B1***), CCK mRNA (magenta, ***A1***, ***B1***), VGluT3 (yellow, ***A2***, ***B2***), and merged (***A3***, ***B3***) in the CA1 region treated with vehicle (***A***) or Endo-N (***B***). Arrows represent VGluT3$^+$ serotonergic boutons making contacts with the soma of VGluT3$^+$/CCK$^+$ cell. ***C***, ***D***, Quadruple fluorescence for PSA-NCAM (cyan, ***C1***, ***D1***), VGluT3 mRNA (green, ***C1***, ***D1***), CCK mRNA (magenta, ***C1***, ***D1***), VMAT2 (yellow, ***C2***, ***D2***), and merged (***C3***, ***D3***) in the CA1 region treated with vehicle (***C***) or Endo-N (***D***). Arrows represent VMAT2$^+$ serotonergic boutons making contacts with the soma of VGluT3$^+$/CCK$^+$ cell. ***E***, ***F***, Triple fluorescence for Sox2 (yellow, ***E1***, ***F1***), DCX (magenta, ***E2***, ***F2***), and S100β (cyan, ***E3***, ***F3***) in the subgranular zone of the dentate gyrus treated with vehicle (***E***) or Endo-N (***F***). ***G***, ***H***, The proportions (%) of VGluT3$^+$ (***G***) and VMAT2$^+$ (***H***) lines around the somata of CCK$^+$ cells in the CA1 region treated with vehicle or Endo-N. ***I–K***, The densities ($\times$1000/mm^3) of Sox2$^+$/DCX$^-$/S100β^- neural stem cells (***I***), Sox2$^-$/DCX$^+$/S100β^- neuronal progenitors (***J***), and Sox2$^+$/DCX$^-$/S100β^+ astrocytes (***K***) in the dentate gyrus treated with vehicle or Endo-N. Data are presented as mean $\pm$ SD (n = 4 mice per group). No significant difference between groups is detected. gcl, granule cell layer; hi, hilus; sgz, subgranular zone. Scale bars: ***D3***, 3 μm (applies to ***A–D***); ***F3***, 10 μm (applies to ***E*** and ***F***).

vehicle-treated mice at bregma –1.94 mm (Fig. 5*J*, Table 1). These findings indicate that a local injection of Endo-N might deplete PSA-NCAM in the CA1 region. Additionally, Endo-N might spread slightly beyond the CA1 region to the dentate gyrus, although the reduction in the PSA-NCAM immunoreactivity in the dentate gyrus seemed limited compared with the CA1 region.

Digestion of PSA-NCAM in the CA1 region affects neither the serotonergic terminals nor the adult hippocampal neurogenesis in the dentate gyrus

We wanted to understand the potential effects of local injection of Endo-N into the CA1 region on the serotonergic terminals and adult hippocampal neurogenesis (Fig. 6). To this end, we first examined the patterns of distribution of VGluT3$^+$ serotonergic boutons (Fig. 6*A*,*B*) and VMAT2$^+$ serotonergic boutons (Fig. 6*C*,*D*) around VGluT3$^+$/CCK$^+$ cells in the CA1 region. In general, the distributions of VGluT3$^+$ serotonergic boutons and VMAT2$^+$ serotonergic boutons were similar between vehicle-treated mice and Endo-N-treated mice. The line profile analysis demonstrated that Endo-N injection did not affect the proportions (%) of VGluT3$^+$ lines and VMAT2$^+$ lines around VGluT3$^+$/CCK$^+$ cells (Fig. 6*G*,*H*, Table 1). These findings indicate that the local injection of Endo-N might not affect the distributions of serotonergic terminals.

Because Endo-N spread slightly into the dentate gyrus, we next examined the potential changes in adult hippocampal neurogenesis in the dentate gyrus. The general distributions of adult neurogenesis markers (Sox2, DCX, and S100β) were comparable between vehicle-treated mice and Endo-N-treated mice (Fig. 6*E*,*F*). The densities ($\times$1000/mm^3) of Sox2$^+$/DCX$^-$/S100β^- neural stem cells, Sox2$^-$/DCX$^+$/S100β^- neuronal progenitors, and Sox2$^+$/DCX$^-$/S100β^+ astrocytes were not affected by Endo-N injection into the CA1 region (Fig. 6*I–K*, Table 1). These results ruled out the possibility that local injection of Endo-N into the CA1 region might result in the modulation of adult hippocampal neurogenesis in the dentate gyrus.

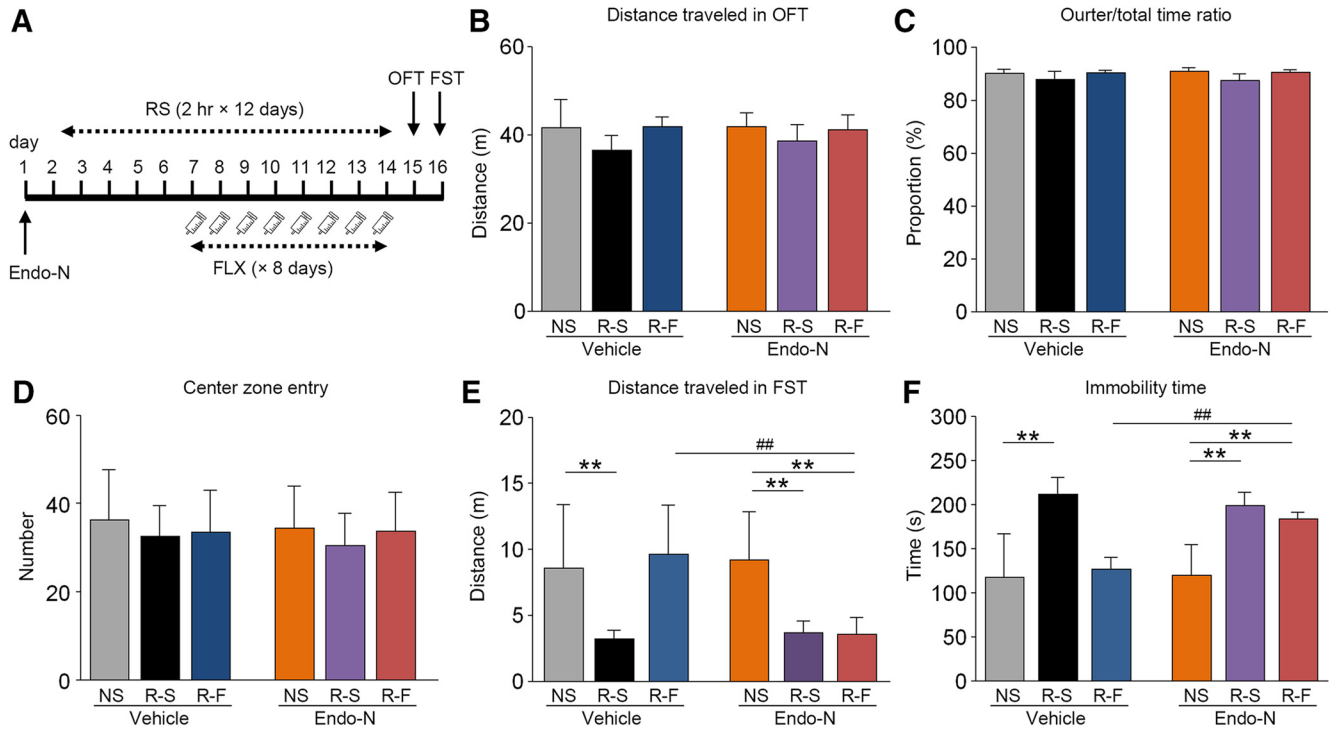

Figure 7. Digestion of PSA-NCAM in the CA1 region does not result in depression-related behavior but impairs antidepressant efficacy. ***A***, The schedule of Endo-N injection, exposure to restraint stress (RS), treatment with fluoxetine (FLX), open field test (OFT), and forced swim test (FST). ***B***, The distance traveled (in meters, m) during the open field test. ***C***, The proportions (%) of time spent in the outer zone in total time during the open field test. ***D***, The number of entries into the center zone during the open field test. ***E***, The total distance traveled (m) during the forced swim test. ***F***, The immobility time (in seconds, s) during the forced swim test. Data are presented as mean ± SD ($n = 10$ mice per group). Statistical significance is represented as follows: $^{**}p < 0.01$ (effect of stress and/or FLX); $^{\#\#}p < 0.01$ (effect of Endo-N).

Digestion of PSA-NCAM in the CA1 region impairs the antidepressant efficacy

Several preclinical studies indicate that serotonergic neurotransmission in the hippocampus may play a key role in mediating the therapeutic actions of antidepressants (Dale et al., 2016). We thus aimed to determine the potential involvement of PSA-NCAM in the hippocampus for the efficacy of antidepressant FLX (Fig. 7*A*). We first examined the effects of Endo-N injection versus stress and FLX treatment in the open field test by two-way ANOVA (Fig. 7*B–D*, Table 3). There was no effect of Endo-N injection on the distance traveled in the open field test (Fig. 7*B*). Restraint stress and FLX treatment did not affect the distance traveled either. The thigmotaxis estimated from the outer/total time ratios (%) was not affected by Endo-N injection (Fig. 7*C*). Restraint stress and FLX treatment did not affect the ratios, either. Similarly, the number of center zone entries was not affected by Endo-N injection, restraint stress, and FLX treatment (Fig. 7*D*). These results indicate that the digestion of PSA-NCAM in the CA1 region affects neither the locomotor activity nor the thigmotaxis.

We next examined the potential effects of Endo-N injection versus stress and FLX treatment in a forced swim test by two-way ANOVA (Fig. 7*E*,*F*, Table 3). In mice that received a vehicle injection, the distance traveled was reduced by exposure to the restraint stress and restored by FLX treatment (Fig. 7*E*). Injection of Endo-N impaired the recovery of the distance traveled by FLX treatment in mice subjected to the restraint stress. The immobility time increased with exposure to the restraint stress and reduced by the FLX treatment in vehicle-treated mice (Fig. 7*F*). However, the recovery effect of FLX on the immobility time was impaired by injection of Endo-N. These data indicate that PSA-NCAM in the CA1 region may be required for the efficacy of antidepressants.

Restraint stress and an antidepressant alters the expression of PSA-NCAM

We aimed to elucidate the effects of restraint stress and FLX treatment on the expression of PSA-NCAM in the CA1 region (Fig. 8*A–D*). The immunoreactivity for PSA-NCAM was slightly reduced by exposure to the restraint stress, recovered by the FLX treatment, and depleted by an Endo-N injection (Fig. 8*A1–D1*). The general distribution patterns of VGluT3$^+$/CCK$^+$ cells were comparable between all groups (Fig. 8*A2–D2*).

We then quantitatively examined the effects of the restraint stress and FLX treatment on the patterns of expression of PSA-NCAM and CCK in the CA1 region (Fig. 8*E–H*, Table 2). The single-cell fluorescence intensity analysis showed that the intensities (arbitrary unit, a.u.) for PSA-NCAM decreased by exposure to the restraint stress and were restored by the FLX treatment (Fig. 8*E*). However, the densities ($\times 1000/mm^3$) of PSA-NCAM$^+$ cells were not affected by stress exposure and FLX treatment (Fig. 8*F*). These findings indicate that restraint stress and antidepressants may affect the expression of PSA-NCAM.

For confirmation, the potential alterations in the densities ($\times 1000/mm^3$) of VGluT3$^+$ cells/CCK$^+$ cells were examined using the same animals. In both vehicle-treated (Fig. 8*G*) and Endo-N-treated (Fig. 8*H*) mice, there were no differences in the densities of VGluT3$^+$/CCK$^+$ cells by exposure to restraint stress and FLX treatment. These results show that neither restraint stress nor antidepressants may affect the distributions of VGluT3$^+$/CCK$^+$ cells.

To further understand the alterations in PSA-NCAM expression, we performed a Western blot and qRT-PCR (Fig. 8*I–L*, Table 2). The band intensities of PSA-NCAM appeared to be reduced by the restraint stress and slightly recovered by the FLX treatment (Fig. 8*I*). The densitometric analysis showed that the

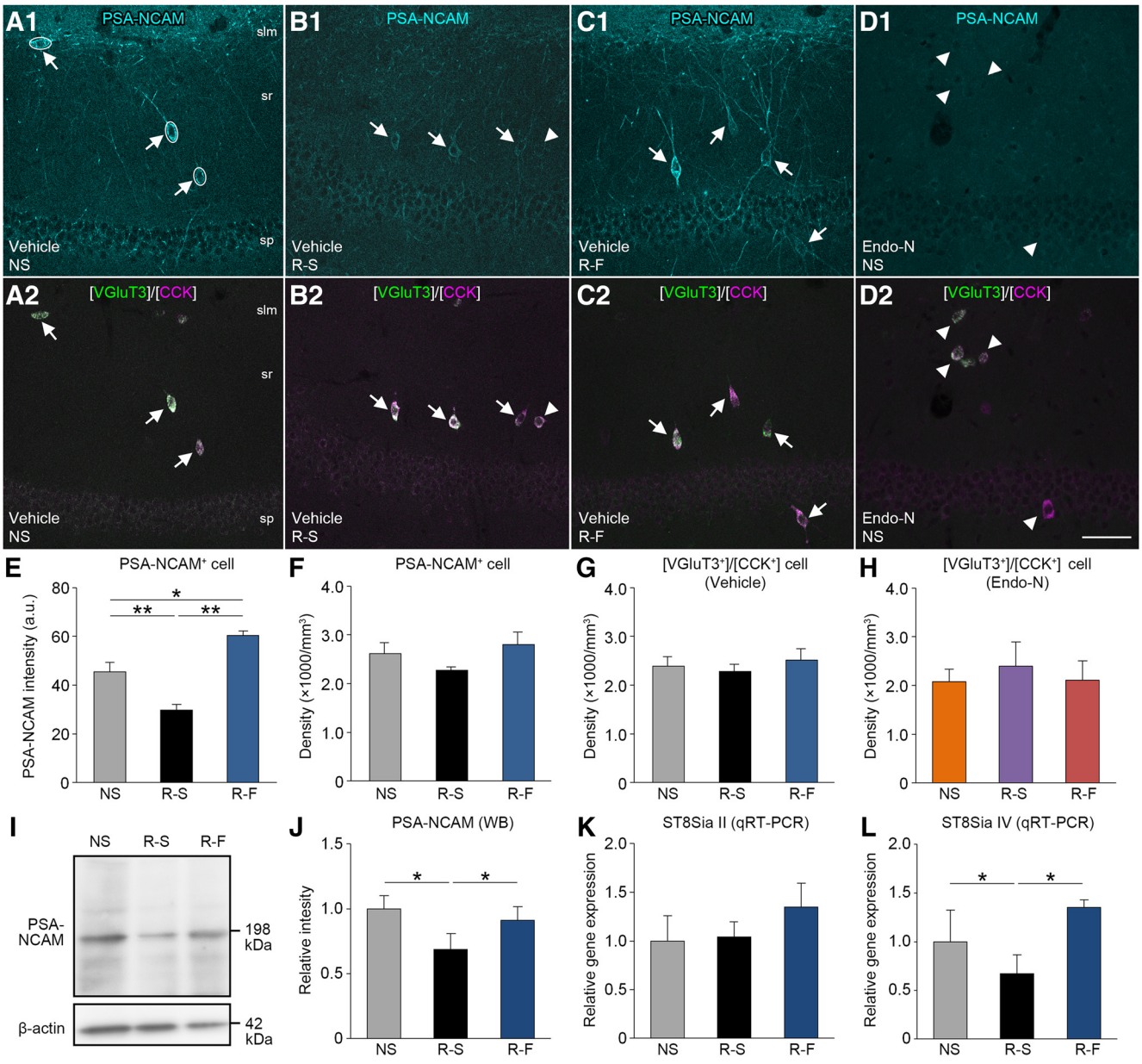

Figure 8. Alterations in PSA-NCAM expression in the CA1 region by exposure to restraint stress and treatment with an antidepressant. ***A–D***, Triple fluorescence for PSA-NCAM (cyan, ***A1–D1***), VGluT3 mRNA (green, ***A2–D2***), and CCK mRNA (magenta, ***A2–D2***) in the CA1 region treated with vehicle (***A–C***) or Endo-N (***D***). Markers enclosed in brackets denote mRNAs detected by FISH. Ellipses circumscribing the somata (in ***A1***) show the examples of single-cell fluorescence intensity analysis. Arrows represent PSA-NCAM $^{+}$/VGluT3^{+}/CCK $^{+}$ cells, and arrowheads represent PSA-NCAM $^{-}$/VGluT3^{+}/CCK $^{+}$ cells. ***E***, ***F***, The fluorescence intensities (arbitrary unit, a.u., ***E***) and the densities ($\times$1000/mm^{3}, ***F***) of the total PSA-NCAM $^{+}$ cells. ***G***, ***H***, The densities ($\times$1000/mm^{3}) of VGluT3 $^{+}$/CCK $^{+}$ cells in the CA1 region treated with vehicle (***G***) or Endo-N (***H***). ***I***, Western blot for PSA-NCAM in the CA1 region. ***J***, The fold differences (relative to nonstressed controls) in protein concentrations of PSA-NCAM as measured by Western blot densitometry (WB). ***K***, ***L***, The fold differences (relative to nonstressed controls) in gene expression of ST8Sia II (***K***) and ST8Sia IV (***L***) determined by qRT-PCR. Data are presented as mean ± SD ($n = 5$ mice per group in ***E***, $n = 4$ mice per group in ***F–H***, ***J–L***). Statistical significance is represented with asterisk: *$p < 0.05$; **$p < 0.01$. slm, stratum lacunosum-moleculare; sp, stratum pyramidale; sr, stratum radiatum. Scale bar in ***D2***, 50 μm (applies to ***A–D***).

expression of PSA-NCAM was reduced by the restraint stress, which was then restored by FLX treatment (Fig. 8*J*). We then examined the gene expression of two polysialyltransferases, ST8Sia II and IV (Kojima et al., 1997), by qRT-PCR. The expression of ST8Sia II mRNA was neither affected by the restraint stress nor the FLX treatment (Fig. 8*K*). In contrast, the expression of ST8Sia IV mRNA was reduced by the restraint stress and recovered by the FLX treatment (Fig. 8*L*). These findings suggest that ST8Sia IV may be involved in the alterations in the expression of PSA-NCAM in response to stress exposure and antidepressant treatment.

Digestion of PSA-NCAM impairs the enhancement of serotonergic signaling by an antidepressant.

Prior research has shown that the expression of p11 may be involved in serotonergic signaling and the efficacy of antidepressants (Svenningsson et al., 2013). To understand whether PSA-NCAM may be involved in p11 expression, we examined the effects of Endo-N injection, restraint stress, and FLX treatment on expression of p11 in the CA1 region by immunostaining (Fig. 9*A–D*). We considered that quantification of relative staining intensities could be amenable; thus, we performed the single-cell fluorescence intensity analysis and compared the effects of

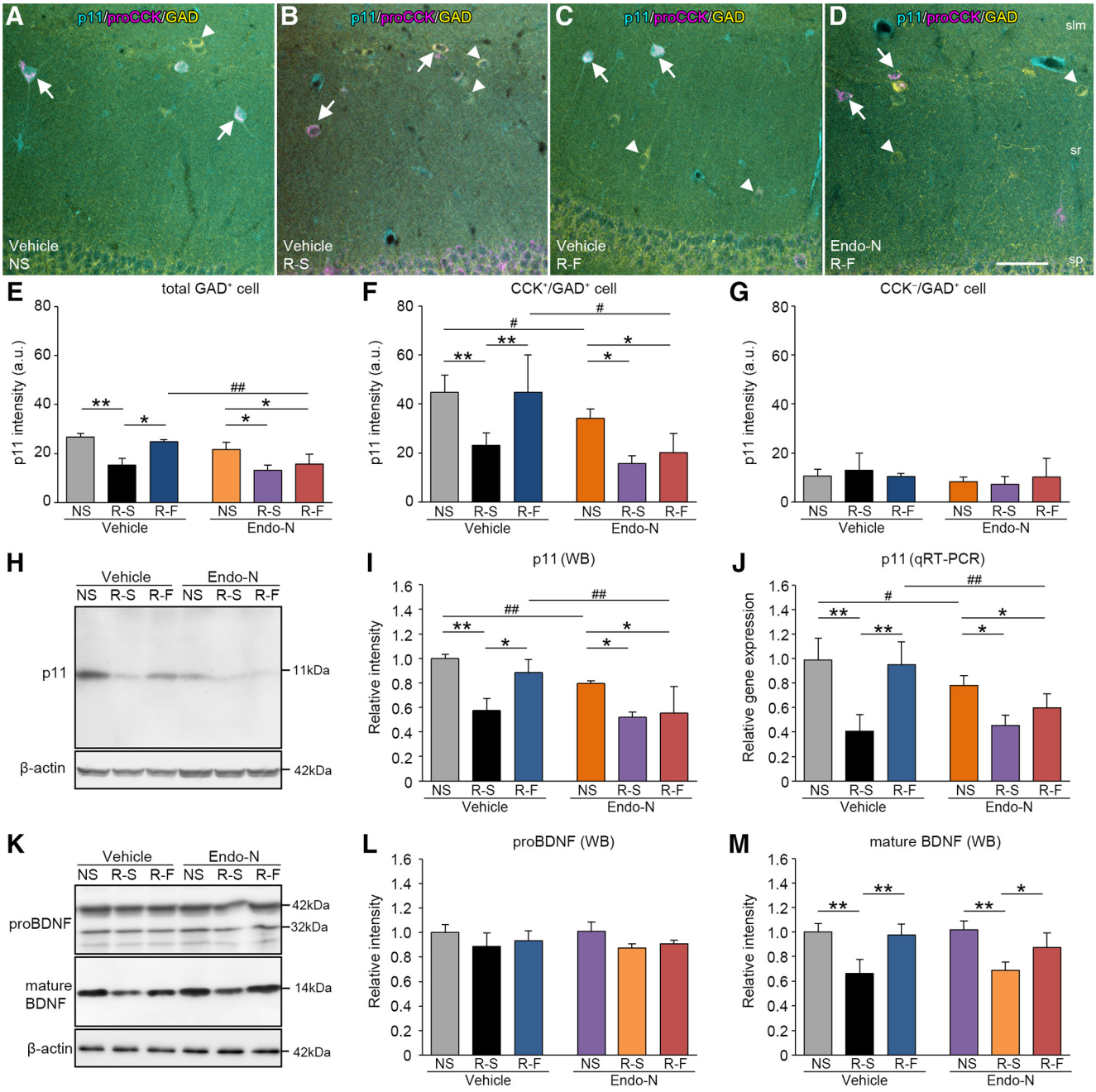

Figure 9. Digestion of PSA-NCAM in the CA1 region impairs the enhancement of expression of p11 by an antidepressant. ***A–C***, Triple fluorescence for p11 (cyan), proCCK (magenta), and GAD (yellow) in the CA1 region treated with vehicle (***A–C***) or Endo-N (***D***). Arrows represent proCCK $^{+}$/GAD $^{+}$ cells, and arrowheads represent proCCK $^{-}$/GAD $^{+}$ cells. ***E–G***, The intensities (arbitrary unit, a.u.) of p11 in the total GAD $^{+}$ cells (***E***), proCCK $^{+}$/GAD $^{+}$ cells (***F***), and proCCK $^{-}$/GAD $^{+}$ cells (***G***). ***H***, Western blot for p11 in the CA1 region. ***I***, The fold differences (relative to nonstressed controls) in protein concentrations of p11 as determined by Western blot densitometry (WB). ***J***, The fold differences (relative to nonstressed controls) in gene expression of p11 determined by qRT-PCR. ***K***, Western blot for proBDNF and mature BDNF in the CA1 region. ***L***, The fold differences (relative to nonstressed controls) in protein concentrations of proBDNF as measured by Western blot densitometry. ***M***, The fold differences (relative to nonstressed controls) in protein concentrations of mature BDNF as measured by Western blot densitometry. Data are presented as mean ± SD (n = 3 mice per group in ***E–G***, n = 4 mice per group in ***I***, ***J***, ***L***, and ***M***). Statistical significance is represented as follows: $^{*}p < 0.05$, $^{**}p < 0.01$ (effect of stress and/or FLX); $^{\#}p < 0.05$, $^{\#\#}p < 0.01$ (effect of Endo-N). slm, stratum lacunosum-moleculare; sp, stratum pyramidale; sr, stratum radiatum. Scale bar in ***D***, 50 μm (applies to ***A–D***).

Endo-N injection versus stress or FLX treatment (Fig. 9*E–G*, Table 3). We first examined the intensities of p11 in total GAD $^{+}$ cells and found that the restraint stress reduced them and the FLX treatment restored them in vehicle-treated mice (Fig. 9*E*). However, the recovery effects of FLX on p11 expression was inhibited by injection of Endo-N. We next examined the intensities of p11 in proCCK $^{+}$/GAD $^{+}$ cells and obtained comparable results (Fig. 9*F*). By contrast, the fluorescence intensities of p11 in proCCK $^{-}$/GAD $^{+}$ cells were not affected by exposure to restraint stress, nor FLX treatment, nor Endo-N injection (Fig. 9*G*). These data indicate that PSA-NCAM may be involved in elevating p11 expression in CCK $^{+}$ cells by antidepressants.

To confirm the involvement of PSA-NCAM in p11 expression, we performed a Western blot and qRT-PCR (Fig. 9*H–J*, Table 3). The band intensities of p11 appeared slightly reduced by Endo-N injection (Fig. 9*H*). The densitometric analysis showed

that the expression of p11 was reduced by the restraint stress in vehicle-treated mice, then was restored by the FLX treatment (Fig. 9*I*). As expected, the recovery of p11 expression by FLX treatment was not observed in Endo-N-treated mice. In addition, Endo-N injection lowered the p11 expression in nonstressed controls. Like the results obtained by the Western blot, p11 mRNA expression was reduced by the restraint stress and recovered by FLX in vehicle-treated mice, and Endo-N injection caused a loss of recovery of p11 mRNA expression by the FLX treatment (Fig. 9*J*). An Endo-N injection reduced the expression of p11 mRNA in both the nonstressed controls and FLX-treated mice, which supports the assertion that PSA-NCAM may be required for the elevation of p11 expression by antidepressants.

It has been shown that BDNF may regulate p11 expression, and the antidepressant-like effects of BDNF require the response of p11 (Warner-Schmidt et al., 2010). We thus performed a Western blot to determine whether PSA-NCAM may be involved in the expression of proBDNF and mature BDNF in the CA1 region (Fig. 9*K–M*, Table 3). The band intensities of proBDNF were not affected by Endo-N injection, whereas those of mature BDNF appeared slightly reduced after the restraint stress. (Fig. 9*K*). The densitometric analysis showed that neither restraint stress nor FLX affected the expression of proBDNF (Fig. 9*L*). Unexpectedly, we found that restraint stress reduced the expression of mature BDNF, and FLX recovered the expression in both vehicle-treated and Endo-N-treated mice (Fig. 9*M*). These findings indicate that PSA-NCAM may not be required for the elevation of expression of mature BDNF by antidepressants.

Digestion of PSA-NCAM in the CA1 region does not affect the anxiolytic efficacy

Because previous studies have suggested that CCK^+ cells may be involved in the anxiolytic effects of benzodiazepines (Freund and Katona, 2007), we examined the potential implication of PSA-NCAM in the efficacy of benzodiazepine anxiolytic DZP using the fear conditioning test and elevated plus-maze. Fear-potentiated behavior in the elevated plus-maze may be a valuable measure for understanding the action of anxiolytics (Korte and De Boer, 2003). Mice received an injection of vehicle or Endo-N into the CA1 region and were then exposed to three trials of a combination of tone (CS) and foot shock (US) in the conditioning box (Fig. 10*A*). On the eighth and ninth day after the injection, contextual fear memory retention was tested with the conditioning context (context A), a novel context (context B), and CS. Mice were then subjected to the elevated plus-maze test the next day.

A similar gradual increase in the freezing time during memory acquisition was seen in the vehicle or Endo-N-treated mice (Fig. 10*B*, Table 1). We then examined the effects of Endo-N injection versus DZP treatment by two-way ANOVA (Fig. 10*C–G*, Table 3). There was no effect of Endo-N injection on the contextual fear memory in mice treated with saline or vehicle (Fig. 10*C*). Administration of DZP reduced the contextual fear memory in both vehicle-mice and Endo-N-treated mice. Neither Endo-N injection nor DZP treatment affected the freezing time in the nonconditioning context (Fig. 10*D*). There was no effect of Endo-N injection on the cued fear memory in mice treated with saline or vehicle (Fig. 10*E*). DZP treatment reduced the cued freezing time in both groups.

Injection of Endo-N did not affect the proportions (%) of open arm entry time in the elevated plus-maze, although this was increased by DZP treatment (Fig. 10*F*). The numbers of open arm entry also showed the lack of effect of Endo-N injection on the efficacy of DZP (Fig. 10*G*). These results indicate that PSA-NCAM may not be required for the anxiolytic efficacy.

Discussion

To summarize the salient findings of this study; the vast majority of $VGluT3^+/CCK^+$ cells were colocalized with PSA-NCAM, whereas most of the VIP^+/CCK^+ cells lacked PSA-NCAM in the CA1 region of the mouse hippocampus. Further, the somata of PSA-$NCAM^+/CCK^+$ cells were highly innervated by serotonergic boutons than that of the PSA-$NCAM^-/CCK^+$ cells; and the expression ratios of 5-HT_{3A} receptors and p11, a serotonin receptor-interacting protein, were higher in PSA-$NCAM^+/CCK^+$ cells than in PSA-$NCAM^-/CCK^+$ cells. Additionally, the efficacy of antidepressant FLX, but not anxiolytic DZP, was impaired by digestion of PSA-NCAM; and the FLX-induced increase in p11 expression was inhibited following PSA-NCAM digestion. Collectively, PSA-NCAM colocalized with $VGluT3^+/CCK^+$ cells may play a unique role in regulating the antidepressant efficacy via the serotonergic pathway.

PSA-NCAM and $VGluT3^+/CCK^+$ cells receiving serotonergic boutons

Until now, CCK^+ cells have been divided into $VGluT3^+/CCK^+$ cells and VIP^+/CCK^+ cells (Somogyi et al., 2004). However, the functional difference between the two subtypes of CCK^+ cells remains somewhat unexplained. The present combined FISH and immunohistochemistry showed that PSA-NCAM in the CA1 region of the mouse hippocampus was highly colocalized with $VGluT3^+/CCK^+$ cells, whereas it was rarely colocalized with VIP^+/CCK^+ cells. To the best of our knowledge, this is the first study showing that PSA-NCAM may be a novel molecular marker that discriminates $VGluT3^+/CCK^+$ cells from VIP^+/CCK^+ cells in the hippocampus.

The present results showed that $VMAT2^+/VGluT3^+$ serotonergic boutons highly innervated $VGluT3^+/CCK^+$ cells colocalized with PSA-NCAM than CCK^+ cells that lacked PSA-NCAM. In addition, the expression ratios of 5-HT_{3A} receptors and p11, a serotonin receptor-interacting protein, were higher in PSA-$NCAM^+/CCK^+$ cells than in PSA-$NCAM^-/CCK^+$ cells. Earlier studies have demonstrated that CCK^+ cells in the hippocampus receive dense serotonergic raphe-hippocampal fibers (Miettinen and Freund, 1992; Papp et al., 1999). It has also been shown that VGluT3, coexisting with $VMAT2^+$ synaptic terminals, actively promotes the serotonergic release in the raphe–hippocampus system (Amilhon et al., 2010). Interestingly, $VGluT3^+/CCK^+$ cells are shown to specifically innervate calbindin-expressing CA1 pyramidal neurons that project to the contralateral entorhinal cortex (Varga et al., 2010). Therefore, we hypothesize that $VGluT3^+/CCK^+$ cells may be involved in relaying information from the raphe nuclei to the contralateral entorhinal cortex.

Previous studies reported that p11 was colocalized with 5-HT_{1B} receptors and 5-HT_{4B} receptors in the hippocampus (Egeland et al., 2010). In this study, we found that a substantial population of CCK^+ cells expressed p11 in the hippocampus. Further, the expression ratios of p11 were higher in 5-HT_{3A} receptor$^+/CCK^+$ cells than in the 5-HT_{3A} receptor$^-/CCK^+$ cells. It has been shown that p11 plays a vital role in the regulation of 5-HT receptor-mediated emotional processing in the hippocampus, but the cell types involved in the action of p11 remain to be elucidated (Svenningsson et al., 2013). The expression of p11 mRNA was downregulated in both animal models of depression and patients suffering from depression (Svenningsson et al., 2006). Antidepressants, as well as electroconvulsive shock, in-

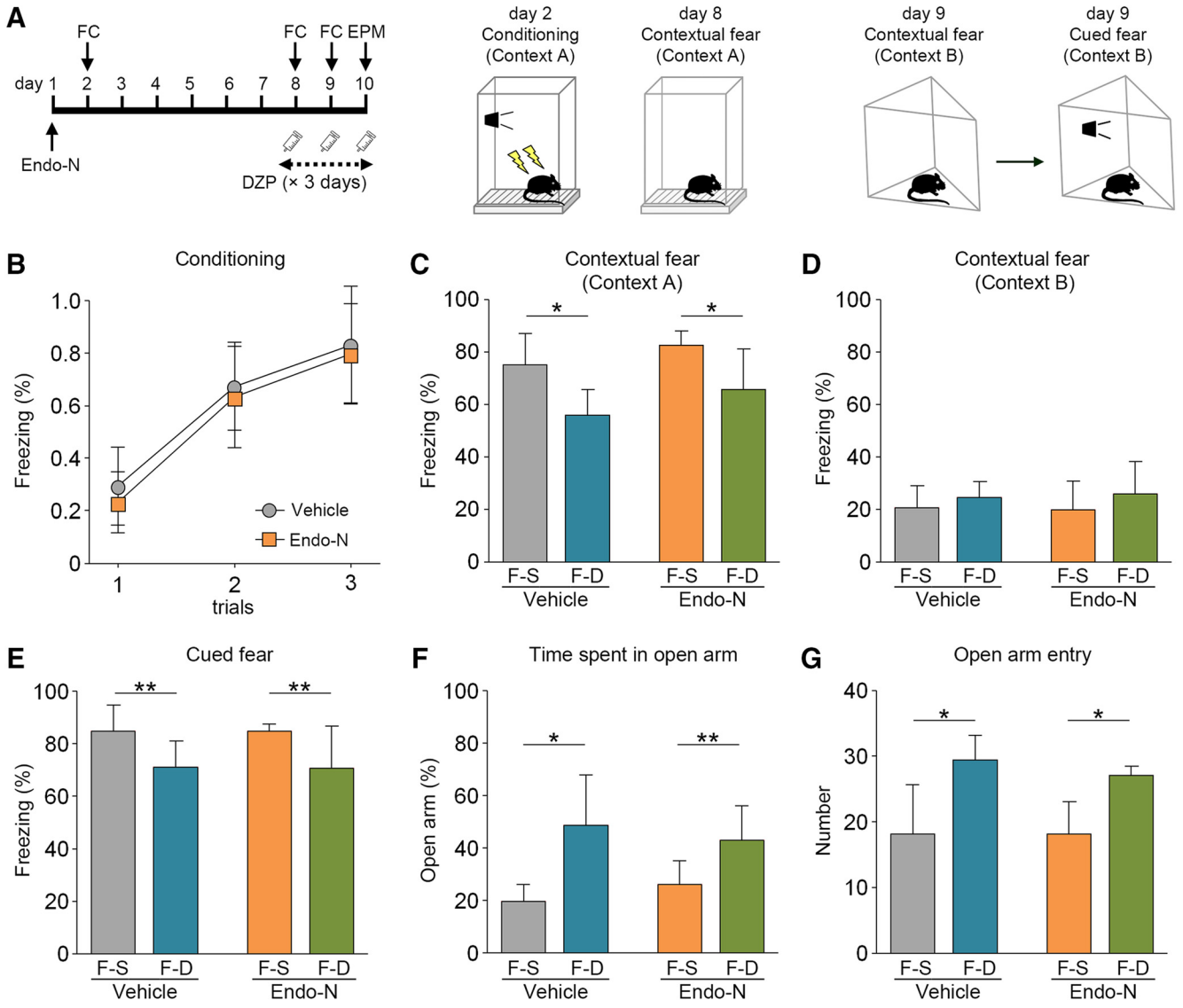

Figure 10. Digestion of PSA-NCAM in the CA1 region affects neither contextual fear memory nor anxiolytic efficacy. ***A***, The schedule of injection of Endo-N, fear conditioning (FC), elevated plus-maze (EPM) test, and administration of diazepam (DZP). ***B***, On the second day, mice that had received an injection of vehicle (gray circle) or Endo-N (orange square) into the CA1 region are conditioned by three tone-foot shock trials in context A. ***C***, The proportions (%) of time spent in freezing behavior in context A. ***D***, ***E***, The proportions (%) of time spent in freezing behavior in context B (***D***) and those during the cue presentation period (***E***). ***F***, ***G***, The proportions (%) of time staying on the open arm (***F***) and the numbers of entries into the open arm (***G***) in elevated plus-maze. Data are presented as mean ± SD ($n = 10$ mice per group). Statistical significance is represented with asterisks: *$p < 0.05$; **$p < 0.01$ (effect of DZP). No significant effect of Endo-N is detected.

creased the expression of p11 mRNA and p11 protein in the mouse hippocampus (Warner-Schmidt et al., 2010). The learned helplessness procedure caused depression-related behaviors in mice, leading to a decline in the expression of the 5-HT_{2A} receptor and p11 in the hippocampus (Sachs et al., 2015). Paired electrophysiological recordings showed that 5-HT_{1B} receptors in CCK^+ cells in the hippocampus were not functional in p11-null mice (Medrihan et al., 2017). In this study, we found that the expression of p11 in the hippocampus was downregulated by the restraint stress and upregulated by FLX. Interestingly, the digestion of PSA-NCAM inhibited the FLX-induced upregulation of p11 expression. Our results indicate that PSA-NCAM colocalized with $VGluT3^+/CCK^+$ cells may be essential for the increase in p11 expression by antidepressants.

PSA-NCAM and depression-related behavior

Earlier research showed that both ST8Sia II and ST8Sia IV play dominant roles in the formation of PSA-NCAM (Kojima et al., 1997). In this study, we found that the expressions of ST8Sia IV in the CA1 region decreased when exposed to restraint stress and increased with FLX treatment, whereas the expression of ST8Sia II was not affected by restraint stress or FLX. Previous studies have shown that serotonergic neurotransmission, antidepressants, and depression may be implicated in the expression of PSA-NCAM in several brain areas. For instance, the expression of PSA-NCAM was reduced in the basal ganglia regions, hypothalamic nuclei, and hippocampus after serotonergic lesion following 5,7-dihydroxytryptamine (5,7-DHT) injections into the dorsal and medial raphe nuclei of adult rats (Brezun and Daszuta, 2000). Chronic administration of the antidepressant FLX increased the expression of PSA-NCAM in the medial prefrontal cortex of adult rats (Varea et al., 2007). A clinical study has shown that the expression of PSA-NCAM, in the basolateral and basomedial amygdala, decreased in depressed patients (Varea et al., 2012). Although ST8Sia II and ST8Sia IV are considered to control the expression of PSA *in vivo* cooperatively, they differen-

tially use N-glycans on different sites of NCAM (Angata and Fukuda, 2003). Together, these findings indicate that ST8Sia IV, but not ST8Sia II, may be involved in alterations in PSA-NCAM formation in response to stress and antidepressants.

PSA-NCAM and antidepressant efficacy

In this study, we found that the expression of mature BDNF in the CA1 region decreased when exposed to restraint stress and increased with FLX treatment. It has been shown that PSA-NCAM directly binds to bioactive molecules involved in the regulation of neural functions such as BDNF (Sato et al., 2016) and fibroblast growth factor-2 (FGF2) (Elsayed et al., 2012). Based on research to date, BDNF is known to play a significant role in the pathophysiology of depression and the efficacy of antidepressants (Björkholm and Monteggia, 2016). For instance, serum BDNF levels were significantly lower in patients with major depression than in healthy controls (Karege et al., 2002). The expression of BDNF mRNA was reduced in the hippocampus of individuals who have been diagnosed with mood disorders (Thompson Ray et al., 2011). Single nucleotide polymorphisms (SNPs) have been identified in the *BDNF* gene of patients with major depression (Hennings et al., 2019). It has also been shown that antidepressants enhance the expression of BDNF in various brain areas (van Calker et al., 2018). Animal experiments showed that BDNF-null mice were resistant to antidepressants in the forced swim test (Saarelainen et al., 2003). Interestingly, the phosphorylation of the BDNF receptor, tyrosine receptor kinase B (TrkB), and thus BDNF signaling, was reduced in NCAM-null mice that exhibited the depression-related phenotype (Muller et al., 1996). However, it should be noted that PSA does not produce BDNF, but releases previously bound BDNF (Sumida et al., 2015). Our experiment showed that the expression of mature BDNF increased in mice treated with Endo-N and FLX, although the expression of p11 decreased in the same animals. Together, these findings suggest that PSA-NCAM may not be responsible for producing BDNF, although it is required for BDNF signaling that facilitates the expression of p11 to potentiate the antidepressant efficacy.

The present study showed that the digestion of PSA-NCAM did not affect the efficacy of the benzodiazepine anxiolytic DZP. It has been shown that DZP facilitates GABA mediated postsynaptic inhibitory current (Adamec et al., 1981). The GABA potentiating actions of DZP are seen in the hippocampus, thalamus, hypothalamus, and cortex (Calcaterra and Barrow, 2014). The α2 subunit of $GABA_A$ receptors is considered to be a mediator of the anxiolytic effects of DZP (Löw et al., 2000; Rudolph et al., 2001). Interestingly, the α2 subunit of $GABA_A$ receptors in the hippocampal pyramidal cells is targeted by synapses originating from PV-negative, probably VIP^+/CCK^+ cells (Nyíri et al., 2001). Future research focusing on the functional significance of VIP^+/CCK^+ cells in the hippocampus may contribute to understanding the mechanisms underlying the anxiolytic efficacy.

References

Adamec RE, McNaughton B, Racine R, Livingston KE (1981) Effects of diazepam on hippocampal excitability in the rat: action in the dentate area. Epilepsia 22:205–215.

Adams CE, Fisher RS (1990) Sources of neostriatal cholecystokinin in the cat. J Comp Neurol 292:563–574.

Angata K, Fukuda M (2003) Polysialyltransferases: major players in polysialic acid synthesis on the neural cell adhesion molecule. Biochimie 85:195–206.

Amilhon B, Lepicard E, Renoir T, Mongeau R, Popa D, Poirel O, Miot S, Gras C, Gardier AM, Gallego J, Hamon M, Lanfumey L, Gasnier B, Giros B, El Mestikawy S (2010) VGLUT3 (vesicular glutamate transporter type 3) contribution to the regulation of serotonergic transmission and anxiety. J Neurosci 30:2198–2210.

Armstrong C, Soltesz I (2012) Basket cell dichotomy in microcircuit function. J Physiol 590:683–694.

Beinfeld MC (1983) Cholecystokinin in the central nervous system: a minireview. Neuropeptides 3:411–427.

Björkholm C, Monteggia LM (2016) BDNF - a key transducer of antidepressant effects. Neuropharmacology 102:72–79.

Brezun JM, Daszuta A (2000) Serotonergic reinnervation reverses lesion-induced decreases in PSA-NCAM labeling and proliferation of hippocampal cells in adult rats. Hippocampus 10:37–46.

Calcaterra NE, Barrow JC (2014) Classics in chemical neuroscience: diazepam (Valium). ACS Chem Neurosci 5:253–260.

Castillo-Gómez E, Gómez-Climent MA, Varea E, Guirado R, Blasco-Ibáñez JM, Crespo C, Martínez-Guijarro FJ, Nácher J (2008) Dopamine acting through D2 receptors modulates the expression of PSA-NCAM, a molecule related to neuronal structural plasticity, in the medial prefrontal cortex of adult rats. Exp Neurol 214:97–111.

Cope DW, Maccaferri G, Márton LF, Roberts JD, Cobden PM, Somogyi P (2002) Cholecystokinin-immunopositive basket and schaffer collateral-associated interneurones target different domains of pyramidal cells in the CA1 area of the rat hippocampus. Neuroscience 109:63–80.

Dale E, Pehrson AL, Jeyarajah T, Li Y, Leiser SC, Smagin G, Olsen CK, Sanchez C (2016) Effects of serotonin in the hippocampus: how SSRIs and multimodal antidepressants might regulate pyramidal cell function. CNS Spectr 21:143–161.

Del Pino I, Brotons-Mas JR, Marques-Smith A, Marighetto A, Frick A, Marín O, Rico B (2017) Abnormal wiring of CCK+ basket cells disrupts spatial information coding. Nat Neurosci 20:784–792.

DiFiglia M, Marshall P, Covault J, Yamamoto M (1989) Ultrastructural localization of molecular subtypes of immunoreactive neural cell adhesion molecule (NCAM) in the adult rodent striatum. J Neurosci 9:4158–4168.

Egeland M, Warner-Schmidt J, Greengard P, Svenningsson P (2010) Neurogenic effects of fluoxetine are attenuated in p11 (S100A10) knockout mice. Biol Psychiatry 67:1048–1056.

Elsayed M, Banasr M, Duric V, Fournier NM, Licznerski P, Duman RS (2012) Antidepressant effects of fibroblast growth factor-2 in behavioral and cellular models of depression. Biol Psychiatry 72:258–265.

Freund TF (2003) Interneuron diversity series: rhythm and mood in perisomatic inhibition. Trends Neurosci 26:489–495.

Freund TF, Katona I (2007) Perisomatic inhibition. Neuron 56:33–42.

Gómez-Climent MÁ, Guirado R, Castillo-Gómez E, Varea E, Gutierrez-Mecinas M, Gilabert-Juan J, García-Mompó C, Vidueira S, Sanchez-Mataredona D, Hernández S, Blasco-Ibáñez JM, Crespo C, Rutishauser U, Schachner M, Nacher J (2011) The polysialylated form of the neural cell adhesion molecule (PSA-NCAM) is expressed in a subpopulation of mature cortical interneurons characterized by reduced structural features and connectivity. Cereb Cortex 21:1028–1041.

Gundersen HJ, Jensen EB (1987) The efficiency of systematic sampling in stereology and its prediction. J Microsc 147:229–263.

Gundersen HJ, Bendtsen TF, Korbo L, Marcussen N, Møller A, Nielsen K, Nyengaard JR, Pakkenberg B, Sørensen FB, Vesterby A (1988) Some new, simple and efficient stereological methods and their use in pathological research and diagnosis. Apmis 96:379–394.

Hallenbeck PC, Vimr ER, Yu F, Bassler B, Troy FA (1987) Purification and properties of a bacteriophage-induced endo-N-acetylneuraminidase specific for poly-alpha-2,8-sialosyl carbohydrate units. J Biol Chem 262:3553–3561.

Hennings JM, Kohli MA, Uhr M, Holsboer F, Ising M, Lucae S (2019) Polymorphisms in the BDNF and BDNFOS genes are associated with hypothalamus-pituitary axis regulation in major depression. Prog Neuropsychopharmacol Biol Psychiatry 95:109686.

Jinno S, Kosaka T (2006) Cellular architecture of the mouse hippocampus: a quantitative aspect of chemically defined GABAergic neurons with stereology. Neurosci Res 56:229–245.

Jinno S, Aika Y, Fukuda T, Kosaka T (1998) Quantitative analysis of GABAergic neurons in the mouse hippocampus, with optical disector using confocal laser scanning microscope. Brain Res 814:55–70.

Karege F, Perret G, Bondolfi G, Schwald M, Bertschy G, Aubry JM (2002) Decreased serum brain-derived neurotrophic factor levels in major depressed patients. Psychiatry Res 109:143–148.

Klausberger T, Márton LF, O'Neill J, Huck JH, Dalezios Y, Fuentealba P, Suen

WY, Papp E, Kaneko T, Watanabe M, Csicsvari J, Somogyi P (2005) Complementary roles of cholecystokinin- and parvalbumin-expressing GABAergic neurons in hippocampal network oscillations. J Neurosci 25:9782–9793.

Kojima N, Tachida Y, Tsuji S (1997) Two polysialic acid synthases, mouse ST8Sia II and IV, synthesize different degrees of polysialic acids on different substrate glycoproteins in mouse neuroblastoma Neuro2a cells. J Biochem 122:1265–1273.

Korte SM, De Boer SF (2003) A robust animal model of state anxiety: fear-potentiated behaviour in the elevated plus-maze. Eur J Pharmacol 463:163–175.

Löw K, Crestani F, Keist R, Benke D, Brunig I, Benson JA, Fritschy JM, Rulicke T, Bluethmann H, Mohler H, Rudolph U (2000) Molecular and neuronal substrate for the selective attenuation of anxiety. Science 290:131–134.

McLaughlin RJ, Hill MN, Gorzalka BB (2014) A critical role for prefrontocortical endocannabinoid signaling in the regulation of stress and emotional behavior. Neurosci Biobehav Rev 42:116–131.

Medrihan L, Sagi Y, Inde Z, Krupa O, Daniels C, Peyrache A, Greengard P (2017) Initiation of behavioral response to antidepressants by cholecystokinin neurons of the dentate gyrus. Neuron 95:564–576.e4.

Miettinen R, Freund TF (1992) Convergence and segregation of septal and median raphe inputs onto different subsets of hippocampal inhibitory interneurons. Brain Res 594:263–272.

Morales M, Bloom FE (1997) The 5-HT3 receptor is present in different subpopulations of GABAergic neurons in the rat telencephalon. J Neurosci 17:3157–3167.

Muller D, Wang C, Skibo G, Toni N, Cremer H, Calaora V, Rougon G, Kiss JZ (1996) PSA-NCAM is required for activity-induced synaptic plasticity. Neuron 17:413–422.

Nacher J, Blasco-Ibáñez JM, McEwen BS (2002) Non-granule PSA-NCAM immunoreactive neurons in the rat hippocampus. Brain Res 930:1–11.

Nunzi MG, Gorio A, Milan F, Freund TF, Somogyi P, Smith AD (1985) Cholecystokinin-immunoreactive cells form symmetrical synaptic contacts with pyramidal and nonpyramidal neurons in the hippocampus. J Comp Neurol 237:485–505.

Nyíri G, Freund TF, Somogyi P (2001) Input-dependent synaptic targeting of alpha(2)-subunit-containing GABA(A) receptors in synapses of hippocampal pyramidal cells of the rat. Eur J Neurosci 13:428–442.

Papp EC, Hajos N, Acsády L, Freund TF (1999) Medial septal and median raphe innervation of vasoactive intestinal polypeptide-containing interneurons in the hippocampus. Neuroscience 90:369–382.

Rehfeld JF, Friis-Hansen L, Goetze JP, Hansen TV (2007) The biology of cholecystokinin and gastrin peptides. Curr Top Med Chem 7:1154–1165.

Rudolph U, Crestani F, Möhler H (2001) GABA(A) receptor subtypes: dissecting their pharmacological functions. Trends Pharmacol Sci 22: 188–194.

Rutishauser U (2008) Polysialic acid in the plasticity of the developing and adult vertebrate nervous system. Nat Rev Neurosci 9:26–35.

Saarelainen T, Hendolin P, Lucas G, Koponen E, Sairanen M, MacDonald E, Agerman K, Haapasalo A, Nawa H, Aloyz R, Ernfors P, Castrén E (2003) Activation of the TrkB neurotrophin receptor is induced by antidepressant drugs and is required for antidepressant-induced behavioral effects. J Neurosci 23:349–357.

Sachs BD, Rodriguiz RM, Tran HL, Iyer A, Wetsel WC, Caron MG (2015) Serotonin deficiency alters susceptibility to the long-term consequences of adverse early life experience. Psychoneuroendocrinology 53:69–81.

Sairanen M, O'Leary OF, Knuuttila JE, Castrén E (2007) Chronic antidepressant treatment selectively increases expression of plasticity-related proteins in the hippocampus and medial prefrontal cortex of the rat. Neuroscience 144:368–374.

Sato C, Hane M, Kitajima K (2016) Relationship between ST8SIA2, polysialic acid and its binding molecules, and psychiatric disorders. Biochim Biophys Acta 1860:1739–1752.

Schnaar RL, Gerardy-Schahn R, Hildebrandt H (2014) Sialic acids in the brain: gangliosides and polysialic acid in nervous system development, stability, disease, and regeneration. Physiol Rev 94:461–518.

Seki T (2002) Hippocampal adult neurogenesis occurs in a microenvironment provided by PSA-NCAM-expressing immature neurons. J Neurosci Res 69:772–783.

Somogyi J, Baude A, Omori Y, Shimizu H, El Mestikawy S, Fukaya M, Shigemoto R, Watanabe M, Somogyi P (2004) GABAergic basket cells expressing cholecystokinin contain vesicular glutamate transporter type 3 (VGLUT3) in their synaptic terminals in hippocampus and isocortex of the rat. Eur J Neurosci 19:552–569.

Sumida M, Hane M, Yabe U, Shimoda Y, Pearce OM, Kiso M, Miyagi T, Sawada M, Varki A, Kitajima K, Sato C (2015) Rapid trimming of cell surface polysialic acid (PolySia) by exovesicular sialidase triggers release of preexisting surface neurotrophin. J Biol Chem 290:13202–13214.

Svenningsson P, Chergui K, Rachleff I, Flajolet M, Zhang X, El Yacoubi M, Vaugeois JM, Nomikos GG, Greengard P (2006) Alterations in 5-HT1B receptor function by p11 in depression-like states. Science 311:77–80.

Svenningsson P, Kim Y, Warner-Schmidt J, Oh YS, Greengard P (2013) p11 and its role in depression and therapeutic responses to antidepressants. Nat Rev Neurosci 14:673–680.

Thompson Ray M, Weickert CS, Wyatt E, Webster MJ (2011) Decreased BDNF, trkB-TK+ and GAD67 mRNA expression in the hippocampus of individuals with schizophrenia and mood disorders. J Psychiatry Neurosci 36:195–203.

Umbriaco D, Garcia S, Beaulieu C, Descarries L (1995) Relational features of acetylcholine, noradrenaline, serotonin and GABA axon terminals in the stratum radiatum of adult rat hippocampus (CA1). Hippocampus 5:605–620.

van Calker D, Serchov T, Normann C, Biber K (2018) Recent insights into antidepressant therapy: distinct pathways and potential common mechanisms in the treatment of depressive syndromes. Neurosci Biobehav Rev 88:63–72.

Varea E, Blasco-Ibáñez JM, Gómez-Climent MA, Castillo-Gómez E, Crespo C, Martínez-Guijarro FJ, Nácher J (2007) Chronic fluoxetine treatment increases the expression of PSA-NCAM in the medial prefrontal cortex. Neuropsychopharmacology 32:803–812.

Varea E, Guirado R, Gilabert-Juan J, Martí U, Castillo-Gómez E, Blasco-Ibáñez JM, Crespo C, Nacher J (2012) Expression of PSA-NCAM and synaptic proteins in the amygdala of psychiatric disorder patients. J Psychiatr Res 46:189–197.

Varga C, Lee SY, Soltesz I (2010) Target-selective GABAergic control of entorhinal cortex output. Nat Neurosci 13:822–824.

Warner-Schmidt JL, Chen EY, Zhang X, Marshall JJ, Morozov A, Svenningsson P, Greengard P (2010) A role for p11 in the antidepressant action of brain-derived neurotrophic factor. Biol Psychiatry 68:528–535.

Wong MY, Liu C, Wang SSH, Roquas ACF, Fowler SC, Kaeser PS (2018) Liprin-alpha3 controls vesicle docking and exocytosis at the active zone of hippocampal synapses. Proc Natl Acad Sci U S A 115:2234–2239.

Yamada J, Nakanishi H, Jinno S (2011) Differential involvement of perineuronal astrocytes and microglia in synaptic stripping after hypoglossal axotomy. Neuroscience 182:1–10.

Yamada J, Ohgomori T, Jinno S (2017) Alterations in expression of cat-315 epitope of perineuronal nets during normal ageing, and its modulation by an open-channel NMDA receptor blocker, memantine. J Comp Neurol 525:2035–2049.

Yoshida K, Drew MR, Mimura M, Tanaka KF (2019) Serotonin-mediated inhibition of ventral hippocampus is required for sustained goal-directed behavior. Nat Neurosci 22:770–777.

Zhang X, Andren PE, Greengard P, Svenningsson P (2008) Evidence for a role of the 5-HT1B receptor and its adaptor protein, p11, in L-DOPA treatment of an animal model of parkinsonism. Proc Natl Acad Sci U S A 105:2163–2168.